Cleveland State University
EngagedScholarship@CSU

ETD Archive

Spring 1-1-2020

Pressure-based Impedance Control of A Pneumatic Actuator

John Francis Mohorcic
Cleveland State University

Follow this and additional works at: https://engagedscholarship.csuohio.edu/etdarchive

How does access to this work benefit you? Let us know!

Recommended Citation

Mohorcic, John Francis, "Pressure-based Impedance Control of A Pneumatic Actuator" (2020). *ETD Archive*. 1220.
https://engagedscholarship.csuohio.edu/etdarchive/1220

This Thesis is brought to you for free and open access by EngagedScholarship@CSU. It has been accepted for inclusion in ETD Archive by an authorized administrator of EngagedScholarship@CSU. For more information, please contact library.es@csuohio.edu.

PRESSURE-BASED IMPEDANCE CONTROL OF A PNEUMATIC ACTUATOR

JOHN FRANCIS MOHORCIC

Bachelor of Science in Electrical Engineering

Purdue University

May 2015

Submitted in partial fulfillment of requirements for the degree

MASTER OF SCIENCE in Electrical Engineering

at the

CLEVELAND STATE UNIVERSITY

May 2020

We hereby approve this thesis for

JOHN FRANCIS MOHORCIC

Candidate for the Master of Science in Electrical Engineering degree for the

Department of Electrical Engineering and Computer Science

and the CLEVELAND STATE UNIVERSITY'S

College of Graduate Studies by

Thesis Committee Chairperson, Lili Dong, Ph.D.

Department of Electrical Engineering and Computer Science

Committee Member, Petru Fodor, Ph.D.

Department of Physics

Committee Member, Siu-Tung Yau, Ph.D.

Department of Electrical Engineering and Computer Science

Student's Date of Defense: May 4, 2020

DEDICATION

+JMJ+

To my wife, Amy, and our first little one due July 2020

ACKNOWLEDGMENT

I would like to express my sincere gratitude to Dr. Lili Dong for her continued and invaluable support, guidance, and patience in my work. Her knowledge and problem-solving abilities helped me to develop good engineering research to develop, analyze, and solve complex problems in a systematic way.

I would also like to thank my other committee members, Dr. Petru Fodor and Dr. Siu-Tung Yau, for reviewing my thesis and providing valuable feedback.

I would also like to thank Delta Systems, Inc., my employer, for their dedication to my education. Their financial support and flexibility in scheduling allowed me to complete my degree and better myself.

Next, I would like to thank my family for their support and encouragement along the way. To my Mom, Dad, and brother who provided encouragement to me as I started my master's journey, thank you for everything.

Finally, to my wife, who provided the help and encouragement to me at all hours of the night and day to help me complete my thesis. Her selflessness, even when pregnant, did not go unnoticed or unappreciated. I made it to this point because of you, and cannot wait to share with you the joy that comes with completing this journey.

IMPEDANCE CONTROL OF A PNEUMATIC ACTUATOR

JOHN FRANCIS MOHORCIC

ABSTRACT

In this thesis, three control methods are developed for the impedance control of a linear pneumatic actuator for contact tasks using discrete valves. Linear pneumatic actuators, particularly with discrete valves, utilize compressed air to produce linear motion. It is a low cost and clean system with straightforward implementation compared to other actuators. Impedance control is applied to the pneumatic actuator to regulate not only force and position, but also the relationship between them. Specifically, the impedance control yields a desired air pressure based on the actual and desired positions, velocity, and force of a pneumatic cylinder to drive the dynamics of the actuator system. Three controllers including Active Disturbance Rejection Control (ADRC), Sliding Mode Control (SMC), and Extended State Observer (ESO) based SMC are implemented to control the pressure output of the actuator system. The control goal is to drive the actual pressure output to the desired pressure from the impedance control module despite the presence of parameter variations and external disturbances. The performances of these controllers are compared based on their abilities of regulating position, force, and pressure in contact and non-contact situations, as well as the amount of control efforts that excite the valve to achieve these goals. Simulation results demonstrate that ADRC provides the best solution to accomplish the control goals in terms of accurate tracking of position, effectively regulating impedance in the presence of an object, and requiring the least amount of control effort necessary to excite valves.

TABLE OF CONTENTS

LIST OF TABLES

LIST OF FIGURES

CHAPTER I

INTRODUCTION

Pneumatic positioning systems are a prevalent part of modern automation and robotic systems. They are typically used in non-precise positioning tasks and provide an economic and efficient solution. A pneumatic system consists of an actuator and valve subsystems that work together to produce a force and position output of the actuator. The goal of this thesis is to dynamically control the relationship between the force and position output of the pneumatic positioning system through impedance control. The motivation is to provide a pneumatic system that will be able to successfully interact with an environment through accurate positioning and soft contact with an unexpected object. At the beginning of this thesis, the concept of an actuator and its working principles will be described.

A. Background of Actuators

The historical overview in [1] describes the history of actuators. The first type of cylinder used for motion was developed by Denis Papin, a French physicist and inventor, in the mid 1670's. This cylinder, depicted in Figure 1, used steam for actuation. This cylinder was used in steam engines, which played a major part in the success of the Industrial Revolution. This was improved upon in the 1900's with the development of compressed air and the resulting invention of the pneumatic actuator for use in automobile

braking systems. More recently, electrically operated actuators have been developed to turn electrical signals into motion.

Figure 1: First Steam Powered Cylinder Design [1]

1) Types and Purpose of Actuators: An actuator is a type of transducer that converts an input signal into mechanical motion. This input signal is typically hydraulic, electrical, or pneumatic in nature. These actuators are used in automation and robotic systems as a means for the control system to interact with the environment. The mechanical motion produced can be linear, rotary, and oscillatory. This thesis research will focus on linear actuation, for which the direction of movement will be in the same direction as the sum of all forces on the actuator. There are three main categories of actuators in a system depending on the type of energy source that are used to create the mechanical movement: hydraulic, electric, and pneumatic.

a) Hydraulic actuators: Hydraulic actuators are discussed in depth in [2]. They use a fluid to produce the necessary force on the piston rod. A single acting actuator is depicted in Figure 2, which means that the main means of motion only can move the actuator in one direction; in this case, that is to the left. Some other force generator, very often a spring, is used to return the actuator to its resting position when the fluid is removed. Liquid is used since it is not compressible and therefore can transfer substantial

force to the environment. This is a force of nearly twenty-five times that of a pneumatic actuator. Another advantage is minimal power loss over long transmission distances from the pump to the actuator. However, drawbacks to these actuators include cleanliness and the need for other sub-systems. Fluid leaks can cause a reduction in force transmitted as well as cause damage to surrounding components. The need for reservoirs, motors, pumps, heat exchangers, and noise reduction equipment is also a disadvantage for hydraulic actuators as it not only takes up extra space but can also increase cost in maintenance and spare parts.

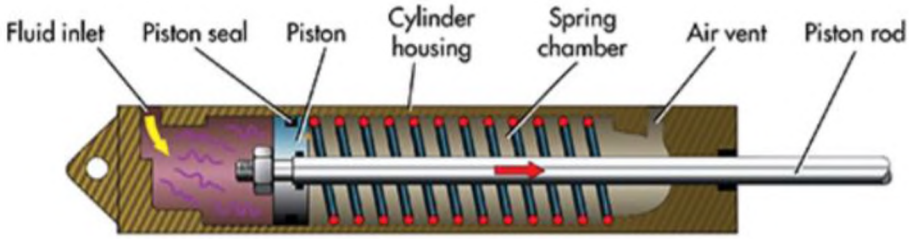

Figure 2: Example of Single Acting Hydraulic Actuator [2]

b) Electric actuator: Figure 3 depicts an example of an electric linear actuator. Using the overview in [2] as a guide to operation, the onboard electronics relate a desired input to a motion output using gears and a ball-screw drive to produce highly accurate moves. In fact, this is the quietest and most accurate type of actuator since the use of onboard electronics provides extreme positioning accuracy and immediate feedback of force and position. The use of motion profiles can be easily executed with various position, torque, and velocity profiles applied over the motion. A major disadvantage to this type of actuator is the high cost of components; it is the costliest of the three types. It is also not suited for all environments and requires the persistence of the motor to hold a position,

thereby causing the motor to overheat over long durations. Depending on the application for which the motor is designed, the force, thrust, and speed limits can become limitations.

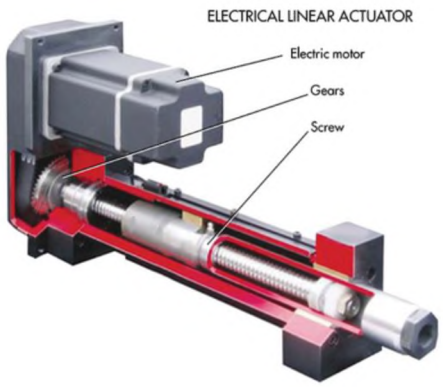

Figure 3: Example of Electric Linear Actuator [2]

c) Pneumatic actuators: Pneumatic actuators provide a suitable compromise between the hydraulic and pneumatic actuators. Since air can be treated like a fluid in some instances, it is like a hydraulic actuator. Although pneumatic actuators can leak like hydraulic actuators, which indeed cause some efficiency issues, they are clean and safe for the environment since leaked air just reenters its surrounding. Air is also not fully incompressible like fluids, so there is some force reduction with pneumatic actuators. However, air's compliance will be used advantageously in the compliance of the actuator with the environment. Pneumatic actuators are also suitable for use in harsh environments. They are simple systems that are low in cost and easy to implement. Although they need a pressure source and its compressor must run continuously, one source can easily accommodate a myriad of machines and other pneumatic equipment.

Pneumatic actuators are typically used in non-precise positioning tasks and provide an economic and efficient solution. These reasons, along with the compliance of air, are mainly why air is chosen as the energy source, instead of other conventional solutions such

as hydraulic or electric energy. However, pneumatic actuators are seldom used in force or precise positioning tasks due to the non-linearity of air flow and compressibility of air. Recent work in non-linear modeling and control of pneumatic actuators and valves has allowed for advancement in the area of using pneumatic actuators as force and precise position control devices.

2) Working Principles of a Pneumatic Actuation System: Pneumatic actuators have simple operating principles. Using Figure 4 as a guide, the concepts of extending and retracting the cylinder can be easily deduced. There are two inlet ports on the cylinder that allows fluid to flow into or out of each respective chamber. The piston on the end of the piston rod allows the rod to move based on the pressure applied to it while also isolating the two chambers from each other. If compressed air of some pressure flows into the back chamber, and the front chamber is exhausted, the overall force on the piston will push the assembly forward. A similar action will happen if more pressure flows into the front chamber than the back, except the movement will be in the opposite direction. If the same force is applied to both cylinders, there will be zero net force and thus no movement. It needs to be stressed that the force needs to be the same and not the pressure. The area of

the piston is different in each chamber. Due to the actuator rod on one side, that side will require more pressure to produce the same force.

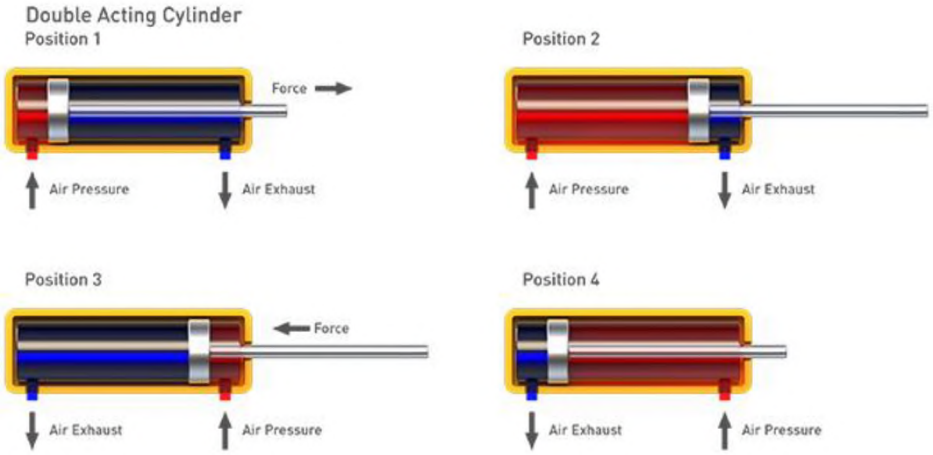

Figure 4: Example of Double Acting Pneumatic Cylinder [3]

Figure 5 is a schematic of a pneumatic actuation system. As can be seen from this example, the cylinder is not the only component that makes up the systems, there is also a valve.

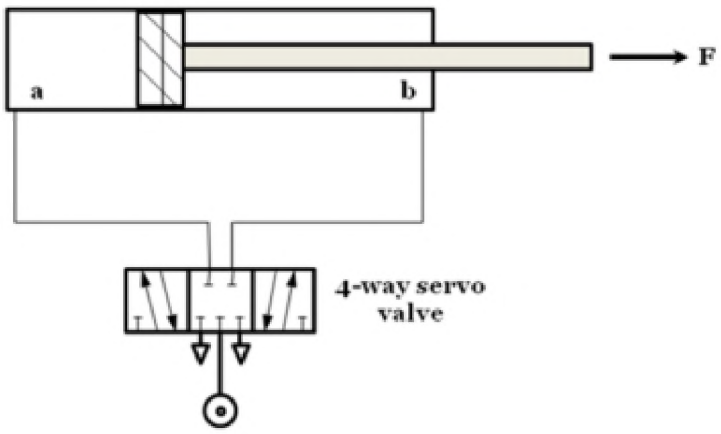

Figure 5: Example Schematic of a Pneumatic Actuation System [4]

Valves are used to regulate the flow of the air into either chamber. The operation of these different valves is described in [5]. Solenoid valves are those types of valves that use an electromagnet to change states. There are five main types of solenoid valves, the uses of which in the control of pneumatic actuators will be described in the ensuing section. The first type of valve is a two-way solenoid valve, which either permits or stops flow from a source. The next type of valve is a three-way valve. This valve has three ports and two orifices. When one orifice is open, the other is typically closed. These are typically used to apply and exhaust pressure from a chamber. The third type is the four-way solenoid valve. This valve has four or five ports, with one being a pressure inlet, and two being outputs to two chambers, and then one for exhausting. These are typically used in controlling double-acting cylinders with one valve. An example of the two-way and three-way valve can be seen in Figure 6. The last two valves are direct-mount and manifold. These are various combinations of the first three types. Some valves are proportional, meaning that the amount the outlet opens is proportional to the inputted electrical signal. Some are full on/off valves, meaning that when a specified voltage is applied the outlet fully opens, otherwise it is fully closed.

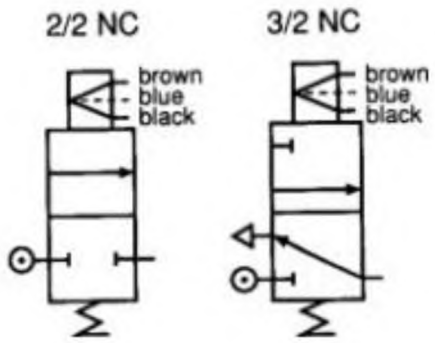

Figure 6: Schematic of a two-way and three-way valve [5]

B. *Components of Pneumatic Actuator System*

The basic operation of the pneumatic actuation system has been described in the previous section. As was elucidated in that section, there are two main subsystems: the actuator and the valve. Now that the basic understanding of the operation of the pneumatic system has been explained, a review of each of these components will now be conducted to provide background into why certain types of cylinders and valves are used in various research settings.

1) Cylinder The typical operation of a double-acting pneumatic cylinder found in Figure 4, the most common type of cylinder, is straight forward. In this typical operation, full pressure is placed on one end of the cylinder and the other end is opened to atmospheric pressure so that the rod moves fully in one direction; the opposite is done for the cylinder to move fully in the other direction. However, to implement a controller for a pneumatic actuator, an accurate model of the system is necessary. As stated in [6], "the most general model for a volume of gas consists of three equations: an equation of state (ideal gas law), the conservation of mass (continuity), and the energy equation". It further explains that this is assuming that the gas is perfect, the pressures and temperature within the chamber are homogeneous, and the kinetic and potential energy terms are negligible. These are reasonable assumptions given the conditions in which pneumatic actuators typically operate. Air is an ideal gas, temperature differences within the system are negligible, and the internal forces of the air pressure on the system tend to be orders of magnitude bigger than the potential and kinetic energies of the system, thus the latter can be ignored. Based on the above information, an accurate equation for the change in pressure of each chamber is formed that considers different heat transfer characteristics for the charging and

discharging process, air compression and decompression, and effective and inactive area within the chambers. The equation provides an accurate model for the pneumatic system. The model takes into consideration effects from small sources such as inactive volume and area differences due to the rod. An almost identical approach is taken in [7] by using mass conservation and thermodynamic energy principles to turn a pneumatic actuator into a force generator for robotic applications. However, this research does not consider the heat transfer, charging and discharging process, air compression, and effective and inactive area within the chamber, as was done in [6]. The experiments carried out in these two papers were not identical, so it is difficult to directly compare the models; however, it is encouraging that a simplified model did provide satisfactory results. This would mean that certain effects and parameters do not need to be exactly known in the model, or that the controller is robust enough to compensate for the absence of these characteristics.

In [8] the model is taken a step further when implementing force dynamics of the piston-payload. Harris expands upon the model in [6] by providing a more precise model for friction. The model used was first developed in [9] and then applied to pneumatic actuators in [10], in which different friction models were used for increasing and decreasing velocity. It was noted in [8] that there was marked improvement in simulation results by implementing this friction along with other factors. This friction model provides a unique approach by dynamically adjusting the friction value based on velocity. Additionally, since this model was implemented with a Programmable Logic Device (PLC), it means that the friction model can be successfully implemented on a real time controller. The problem with this approach is that it is not generalizable, which means that the specific parameters need to be determined for each cylinder used, and there can be

variations between manufacturers, models, and even devices. So, while the friction model may improve position tracking, it would be hard to be accurately implemented as a generalized approach for many devices.

Another possible control problem is the modeling of the system with long transmission lines. Transmission lines are the tubing that connects the valve output to the actuator input. This can be seen in Figure 5 by the solid gray lines that connect both sub-systems. Research in [11] detailed the effect of long transmission lines on a system. The volume of the transmission lines is simply added as part of the cylinder volume, then the volume is divided into four sections, two each for each line. Each line consists of a volume that is half the transmission line and a second section that is the other half of the transmission line plus the cylinder volume. The conclusion of the experiment shows that the approach taken in the paper is valid for transmission lines of 5-10 meters in length. This is due to the forming of a pressure gradient in the transmission tube as well as attenuation formed by the compressibility of air and finite velocity of pressure propagation, causing a time delay. This can be an important factor to consider in controller design given the final layout of the system, especially one that may rely on the system dynamic to calculate force and pressure instead of physical sensors. It should be noted that the volume of these lines is added to the volume of the cylinder, thus effectively only increasing the cylinder volume when there is sufficiently large extra volume in the transmission lines.

2) Valves: Valves are an integral part of the pneumatic system that regulate the control of air into the cylinder. There are many different options and configurations of valves that allow the air to be diverted in various ways depending on the application. This

is typically done with an internal spool that is moved via an electrical or pneumatic actuation. An example of how a spool and land design works is shown in Figure 7.

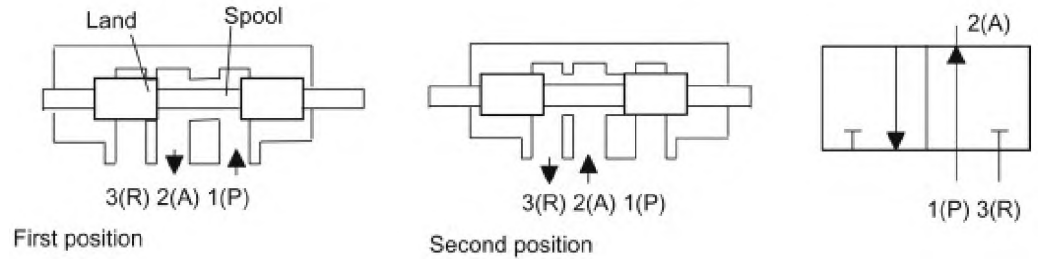

Figure 7: Example of an internal spool [12]

This spool is machined with lands and grooves that open or close specific valves when a signal is provided to divert the air accordingly. This signal can either be an absolute type or proportional type. An absolute signal will move the spool from one position to the next (on/off type). The proportional type will move the spool proportionally to the actuation signal. This allows the air pressure, and thus position of the cylinder, to be proportionally controlled based on the input signal. Both types of control have their advantages and disadvantages, but the main difference is the cost; proportional valves can cost approximately twenty times the price of discrete valves. Examples of proportional spool valves are found in [13] and [14], among others. When using proportional spool valves, the value of the input signal to the valve is directly proportional to the amount the output orifice is opened on the valve. This can then be equated to a mass flow rate of air into the chamber, and in turn can be related to the force and position of the actuator. This is typically used since the value of the control signal can be proportionally related to a percentage of the valve input signal. In contrast, the discrete valve can be modeled based on a pulse-width modulation (PWM) technique for control while regarding the on and off times of the valve as shown in [15] or [16]. Discrete valves use the standard equation for mass flow

through an orifice when the valve is on, and zero flow when the valve is off. The research in [16] uses the PWM technique that successfully controls discrete valves by linearizing the relationship between control signal and velocity of the cylinder. This then allows the discrete valve to create an output that acts as if it were a proportional valve.

C. Applications of Pneumatic Actuators

As stated earlier, pneumatic actuators are used extensively in robotics and automation due to their effective and simple nature. As described in [17], pneumatic actuators are particularly useful for physical system manipulation and rapid motion of objects. Examples of this manipulation include assembly tasks, packing, clamping, and fixing of objects. These tasks are all based on positioning of the actuator. These positioning tasks have developed into four main research areas from [17] that include hardware, system modeling, control of pneumatic positioning systems, and recent trends. These research areas aid in producing industrial technologies that augment the effectiveness and simple nature of the pneumatic actuator while addressing the control challenges of the system to create new and unique industrial devices.

One of the main hindrances of a pneumatic system is the need for compressed air. While compressed air may be common in an industrial setting, it can lend itself to barriers when trying to implement pneumatic actuators in other fields. However, recent work in [18] has developed a pneumatic actuator that does not use an external air source. The application for this soft pneumatic actuator is used in developing virtual reality gloves that provide tactile feedback to the user. This design uses silicone rubber and electrostatic properties to induce an electrostatic attractive force and deform the silicone piece in such a way that tactile feedback is provided to the user's hands. While this is not currently

feasible for use in an industrial setting, which is the goal of this research, it does provide an example of how pneumatic actuators are used in various fields.

Another example of soft robotics and pneumatic systems was detailed in [19]. In this paper, conductive silver ink is printed onto an elastomer substrate to serve as a resistive curvature sensor for the application. Pressure was controlled via pulse-width modulation of solenoid valves, and the pressure was read through sensors at the control board. The outcome was a gripper, created from a set of flexible fingers, that could flex to pick up an object feedback, which is based on pressure input. This paper develops key principles in soft gripping techniques that could be directly applicable to industrial applications, especially those that require the manipulation of delicate parts. While this paper stops short of creating a control system, this would be the logical next step in creating a flexible gripping system.

Energy efficiency of a system becomes of importance if its energy supply is either not infinite or is costly. However, if the system is to become portable, such as in robotics, then the efficiency at which the supply is used becomes of great importance. One way to overcome this problem was discussed above in [18], but this may not be applicable to larger systems that need to move or grip a substantial load. The research in [20] converts the normally wasted exhaust air from a pneumatic system into electric energy. This is achieved by employing a scroll expander to convert the energy into usable electrical power for the system. This could prove to be beneficial in portable robotics, or any system that uses pneumatic energy and is battery powered. The expelled air can then be used to recharge the system batteries to run something like a compressor that creates the necessary pressure for the pneumatic components.

D. Control Problems and Existing Solutions

Now that the background and uses for pneumatic actuation systems have been described, the control problems and solutions can be discussed. There are two main control problems for pneumatic systems. One is related to force and position. Another control problem for these systems is called impedance control. While a full explanation will be provided below, in short, impedance control does not just control either force or position, but the relationship between the two units. As mentioned earlier, a vast majority of pneumatic systems are used for two positions, fully extended and fully retracted. While electric actuation systems can provide position control over the full range of motion, pneumatic actuators tend to be far less expensive. However, controlling the pneumatic system is not a simple task. The nonlinearities of the mass flow rate and valve operation must be taken into careful consideration. This section is divided into two parts. The first sub-section deals with non-impedance control problems and solutions. This will include solutions to either force or position problems. The second section will deal exclusively with impedance control problems and solutions.

1) Position and Force Control Problems: This section will describe the common control problems of pneumatic actuation systems. The three control problems discussed will be position, force and stiffness, and force and position control. These are common control problems when dealing with any of the described actuation systems. Either the position of actuation or the force, or the combination of the two, of the actuation is desired to be controlled.

a) Position control: The first type of control problem for pneumatic actuation systems is probably one of the most common types of control problems for any

system: position control. Position control, by its name, aims to successfully regulate the position of the actuator. As stated earlier, electric actuators do this well. Typically, pneumatic actuators are used for moving an object (or a load) to fully forward and fully backward positions. This is done by applying full pressure to one chamber while venting the other chamber. However, if the position of a pneumatic cylinder were to be controlled through its full range of motion, it could then serve as a reliable alternative to electric actuation. First, pole-placement control in conjunction with self-tuning adaptive control is used in [21] to control the position of a low-friction pneumatic actuator. The model for this control was developed using data from a proportional control method and then calculated using the least squares parameter estimation. While the pole placement technique produced satisfactory results, it was noted that the model did not consider potential system changes, such as temperature, which is why the self-tuning control was added to the system. The recursive least squares method was used to self-tune the system, calculating the parameter vector online. The model was then rebuilt using the plant model, and the coefficients were recalculated using a Diophantine equation. The experimental results show great accuracy after tuning, as well as good position control with the low-friction cylinder. Likewise, a multiple-input single-output nonlinear position control law was developed in [22] using a backstepping methodology. In this paper, the mass flow rate of a proportional valve was modeled by a second order bi-polynomial function, instead of the normal nozzle flow equations. This produced better results in the model. Large tracking errors relative to the movement size in the smaller bore diameter (6.4mm) incurred. The authors contributed this to the ratio of friction force to maximum pneumatic force. The process to obtain the model was unique and could be applied to other valves. Instead of a completely mathematical

approach to finding the mass flow rate, as is normal in similar research, the flow rate for this valve is found using empirical results, and then an equation of best fit was found. In [22], it resulted in a 43% reduction in fitting error versus the normal model. In [23], the position control of a rotary pneumatic actuator for robotics is considered. The position control of this actuator is achieved using pressure sensors and low-cost discrete valves. The position control goal is achieved using a model-based control approach. A novel inverse valve model allows for a faster and more precise pressure control law. The robustness of the system against unknown payloads was also improved with the addition of an augmented estimation algorithm.

b) Force and stiffness control: The other type of control problem with pneumatic actuators is force and stiffness control. Force, based on Newton's second law, is an interaction with a mass that causes it to change its velocity, while stiffness is the tendency of an object to return to its natural position after being subjected to a force. The objective of this controller is to independently and simultaneously control the sum and the difference of the chamber pressures in order to control stiffness and force, respectively. Sliding mode control (SMC) is a common control method for nonlinear systems as it is robust and can account for dynamic uncertainties and nonlinearities. This control method is used in [24] to solve the control problem of simultaneous force and stiffness control of a pneumatic actuator. A pneumatic actuator is used based on the above characteristics of a pneumatic actuator; however, two valves are used in this research, instead of just one, so that the force and stiffness of the system could be controlled independently. The stiffness control is shown in this paper to be the sum of the mass flow rates, and the force dynamics are the difference of the valve commands, and by extension the mass flow rates. Standard

MIMO SMC is then utilized to control the actuator force and stiffness simultaneously. Similarly, a backstepping sliding mode force-stiffness controller is proposed in [14]. For the backstepping-SMC method, a new sliding surface is defined for each step of the backstepping method, and then a SMC is designed for the virtual input of each subsystem. The switching function of the SMC was replaced with a continuous function to facilitate the backstepping. The backstepping method allows for the matched uncertainties condition for SMC to be relaxed and the unmatched uncertainties originating from the thermodynamic equations to remain. Backstepping typically requires high-gain feedback, which makes the system prone to chattering; however, the combination of the SMC and backstepping control mitigates these risks. Using this design, the force and stiffness of the system, which are functions of the chamber pressures and piston position, can be controlled independently. The model was shown to experimentally track the force and stiffness independently with model uncertainties and without chattering. This model provides great tracking ability. The application of backstepping to the SMC controller provides superior tracking when it was compared to a normal SMC. Lastly, a robust SMC for force control is presented in [4], like the other approaches. It should be noted that stiffness is not included in this approach. However, this solution eliminates the need for pressure sensors, and thus contributes to the reduction of cost and complexity of the system. The algorithm uses the simultaneous conditions of the measured actuation force and average air pressure in the actuator to estimate the pressure. The proposal in this research is that since a single four-way valve is used, the pressurizing of one chamber will always be accompanied by the depressurizing of the other chamber. This means that at steady state the average pressure in the system will remain close to a constant value. This constant value is obtained by

analyzing the mass flow into and out of the actuator in steady state. Equating mass flow rate to valve area mathematically yields two equations at which the intersection can be found for a fixed supply pressure that equates to the average pressure. These equations are used to create the typical nonlinear model for a pneumatic system with proportional valve, while including the estimated pressure. The nonlinear model is then used to produce a standard sliding mode controller. This pressure estimation robust force control approach was then successfully experimentally verified. This pressure estimation approach provides a significant advantage in reducing the necessary components for a system, while still being able to track force successfully.

c) *Force and position control*: The goal of force and position control is to regulate the pressure of each chamber of the pneumatic actuator in order to regulate both the position of the piston rod and the force exerted by the piston rod, simultaneously. A similar SMC approach to the force and position control above is used in [25] to guarantee the robustness of the model and the friction and load variations on a teleoperated system. As an attempt at cost reduction, this paper uses PWM to control on/off solenoid-valves instead of servo valves. At a high switching frequency, the discrete signal can be approximated as a continuous input with magnitude determined by the duty cycle. There are seven unique discrete modes of the open loop actuator. This research then designs a time continuous controller based on the averaged model the different modes provide of the system. This then allows SMC to be used for position control of the actuator. In [25], a force relationship was developed for a two-actuator teleoperated setup; however, this was just to provide a proportional force response to the master actuator and not used to control

the force and position relationship, or the impedance of the actuator, as will be described later.

Expanding on on/off valves discussed in [25], On-off valves are again considered in [26], where bilateral control is implemented for force control of a teleoperated system. Hybrid control is used to track the desired force of the system as an inner loop that is then implemented into a four-channel bilateral control architecture that successfully tracks force and position. The control architecture makes it such that four controllers are used to model the dynamics of the system based on linearized dynamics and force and position controller for both the master and slave side. Tuning the four controllers in the communication channel correctly based on these characteristics provides transparent feedback of the system.

2) Impedance Control: The main control problem that will be investigated in this thesis will be that of impedance control. Impedance control is unique in the fact that it regulates both the force and position of the system. However, this is not done independently, but rather by utilizing the relationship between force and position. Impedance control typically requires position as an input and force as an output. Its goal is to simultaneously regulate the relationship between position and force. The impedance control module produces a desired force based on a desired mass-spring-damper model. This force is then correlated to a desired pressure through a system of equations based on the known total pressure in the system, which a controller then uses to regulate the actual pressure. Impedance control was first presented in [27] to control the interaction forces of robotic manipulators, mainly the end-effectors' relationship with the environment. The desired impedance is expressed though the normal spring-mass-damper force equation.

The velocity and position inputs for the spring and damper, respectively, are usually taken as a difference of the desired and current values. This equation is substituted into the typical robot manipulator model that considers the inertia, Coriolis, and friction matrices. This new equation is the control equation that pushes or pulls the manipulator's position toward the specified desired trajectory. A simple derivation of this can be found in [28]. This idea is then expanded upon in [29] by including a force feedback term for use with a peripheral such as a load cell. This term minimizes the deviation of the actual endpoint force from the desired endpoint force. This foundation of how impedance control is implemented on a multi-joint robotic manipulator can then be extrapolated to the pneumatic actuator system by developing and implementing a specific system model.

Impedance control of a pneumatic actuator using discrete solenoid valves is presented in [16]. The control approach is comparable to [25] in that SMC is used for the nonlinear control and PWM is used to control the solenoid valves, but this also implements impedance control. A unique and interesting PWM control, graphed in Figure 8, was used in this research to provide a linear response of the control effort to the velocity of the actuator.

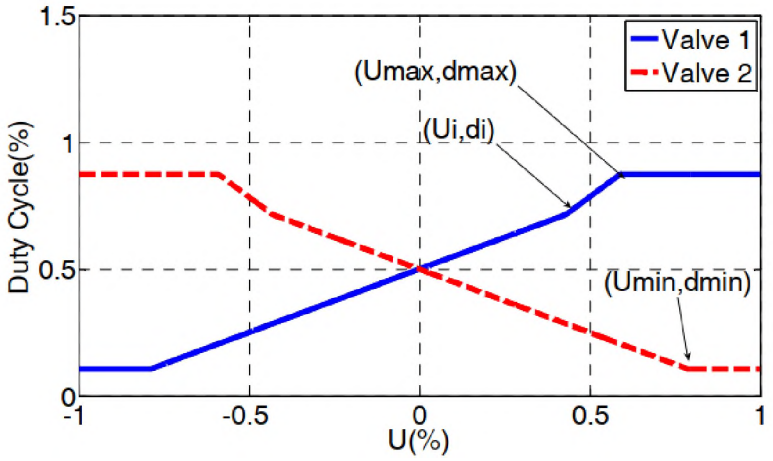

Figure 8: Control Effort Percentage to PWM Duty Cycle for On/Off Valve [16]

The goal of [16] was to understand the control of a pneumatic actuator using on/off valves instead of proportional valves, as stated earlier. This aids in reducing cost. It also investigated the effect of changing the impedance gain on the behavior of the system. The block diagram of the impedance control system is detailed in Figure 9.

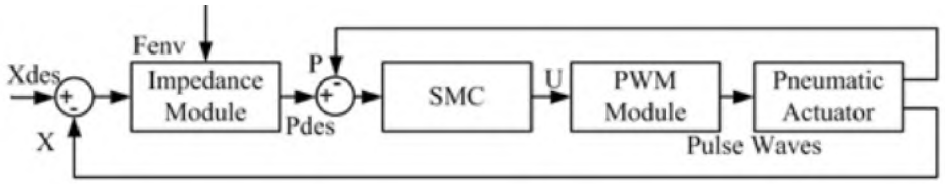

Figure 9: Block Diagram of Impedance Control System for [16]

None of these hypotheses were experimentally proven in this paper, however, the improved control system's simulation results were compared to other papers. The system was able to demonstrate improved position tracking during non-contact phase, as shown with a step and sinusoidal input, and it was also able to apply a controllable contact force in the presence of an obstacle. It was observed that increasing the target stiffness improved the position tracking and the value of the steady state contact force. However, decreasing the

target damping influenced the position tracking of the system, causing greater oscillation; there was no effect on the contact force by changing this parameter.

A hybrid impedance control scheme was presented in [30] to control force and position of a two-link flexible arm robot used in underwater welding applications. The control concept was derived by first creating a bond graph that contains both the controller and physical domain. To achieve better stability due to the uncertainties of underwater conditions, a PID controller along with a passive foundation using impedance control was designed. That is, the base on which the manipulator sits has controllable stiffness, modelled as a mass, spring, and damper system. There are two separate controllers, impedance and PID, along with the passive based model, all coupled through feed-forward gains. The control system allows for the robot stiffness to be low during force control and high during trajectory control. A block diagram of the system can be found in Figure 10. The simulation results provide evidence that the controller will provide good force and position tracking. As seen, the tip follows the correct trajectory until a desired force is observed. At that point the tip holds its position until the force is decreased. This paper does not provide experimental results of the proposed model, just simulation results, so the actual performance of the system is not known. As mentioned in the conclusion, the force tracking ability of the impedance controller was not examined for this research.

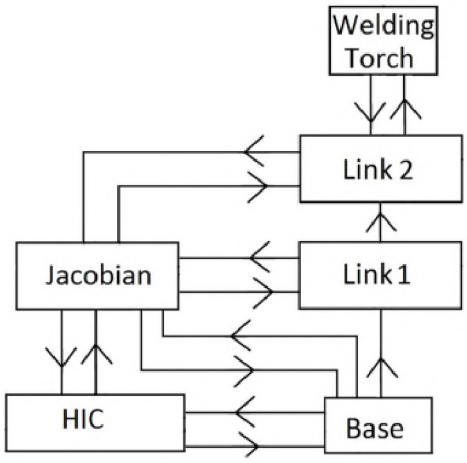

Figure 10: Block Diagram of Hybrid Impedance Controller [30]

Impedance control of a pneumatic actuator is presented in [13] that takes advantage of the natural compliance of pneumatic actuators in such a way that a load cell is not required for force feedback. The motivation for this is to achieve compliant manipulation in assembly tasks. Compliant actuation is a property of an actuator due to the compressibility of air. The impedance controller uses position, velocity, and desired position and velocity to calculate the desired force. This desired force is then passed into the pressure controller which calculates the desired pressure into each valve and commands the proportional valve. These pressures are determined using the standard model for mass flow rate for a compressible gas through a valve. A sliding mode controller is then used to control the pressures. An unconventional choice for the sliding surface was used in this research in that the control influence appears in the first derivative of pressure because it provided better tracking results experimentally. The experimental results show good motion and pressure tracking in free space. The controllable contact forces when transitioning from non-contact to contact tasks were also respectable. An example of pressure and force tracking of the system is graphed in Figure 11. Before contact is made,

the position tracking is acceptable, and then after contact is made the force has a quick impulse before settling to the desired force. This was experimentally verified by driving the system to a position and placing an obstacle in the path at some distance that is less than the desired distance. The force when the actuator encounters the obstacle produces a predictable response based on the target inertia, damping, and stiffness values.

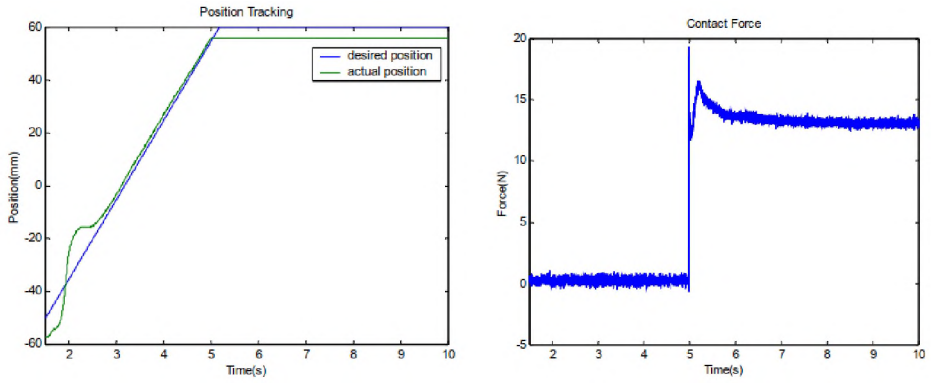

Figure 11: Graph of Position and Force Tracking for [13]

A unilateral teleoperated pneumatic system is implemented in [31] that applies force-based impedance control. Force and position feedback are sent to the impedance controller to maintain the desired force and position on the system. The output of this controller is the desired force of the system based on the designed model. The force error, the difference of the desired and actuating forces, is then inputted into a force controller. The block diagram of the system is shown in Figure 12. While this block diagram includes the slave actuator, the basis of the system is very similar to the control of a non-teleoperated system in [16] shown in Figure 9. In this paper, a SMC is implemented to control the force, which then applies some control force to the teleoperated actuator. The sliding mode controller, chosen because of its robustness to model inaccuracies, was able to effectively track the force of the system, as was shown in the experimental results of it tracking a 20

N and 50 N force. This research provides a direct approach to impedance control that is then applied to a teleoperated actuator successfully.

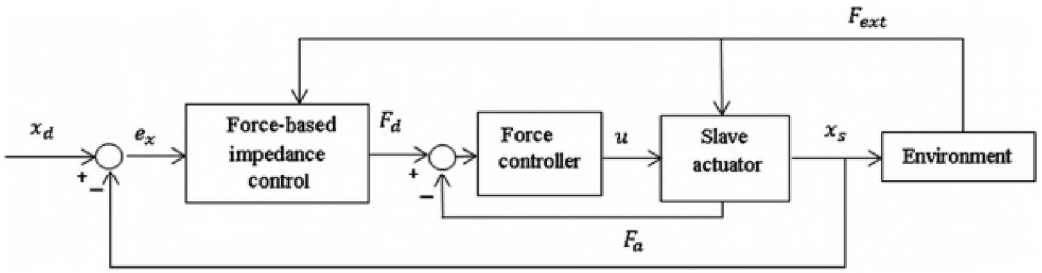

Figure 12: Block Diagram of Force-Based Impedance Control [31]

E. Proposed Control Solution

The proposed control solutions include Active Disturbance Rejection Controller (ADRC), Extended State Observer based Sliding Mode Controller (ESO-based SMC), and SMC which are applied to a linear pneumatic actuator system that contains discrete valves. These controllers are compared based on their performances in regulating piston position, actuator force, and pressure in contact and non-contact situations, in addition to the frequency of excitation signal that they produced for the discrete valves and their robustness against disturbances and system uncertainties. SMC is chosen due to its robustness to deal with uncertainty, and because it only has two tuning parameters. ESO-based SMC is chosen as a control solution due to the high nonlinearity of the problem. The ESO can estimate external disturbances and system states that are not measurable. An additional three parameters are needed for this controller, for a total of five tuning parameters. Lastly, ADRC is chosen as the last controller to compare based on its inclusion of the ESO and its robustness to uncertainty. The ADRC is implemented with limited knowledge of the system model and only two tuning parameters.

F. Contributions of this Thesis

This thesis research focuses on impedance control for pneumatic actuators. Little work has currently been accomplished in this area. In this thesis, ESO-based SMC and ADRC are applied to pressure control for the first time based on the established impedance control module of the actuator. The need for position and velocity feedback of the system is eliminated for pressure control with ESO-based SMC and ADRC. In addition, the implementation of ESO in both of these controllers facilitates the control of the system, even with uncertainties in modeling.

G. Organization of Thesis

This thesis is organized in the following way. In Chapter II, the system model for the pneumatic actuator and valves is presented. In Chapter III, the three controllers are developed, and the stability analyses of three control systems are given. In Chapter IV, the simulation results are demonstrated. Finally, Chapter V concludes the thesis and proposes next steps.

CHAPTER II

MATHEMATICAL MODEL OF THE SYSTEM

A pneumatic system consists of two main parts: the actuator and the valve, as depicted in Figure 13.

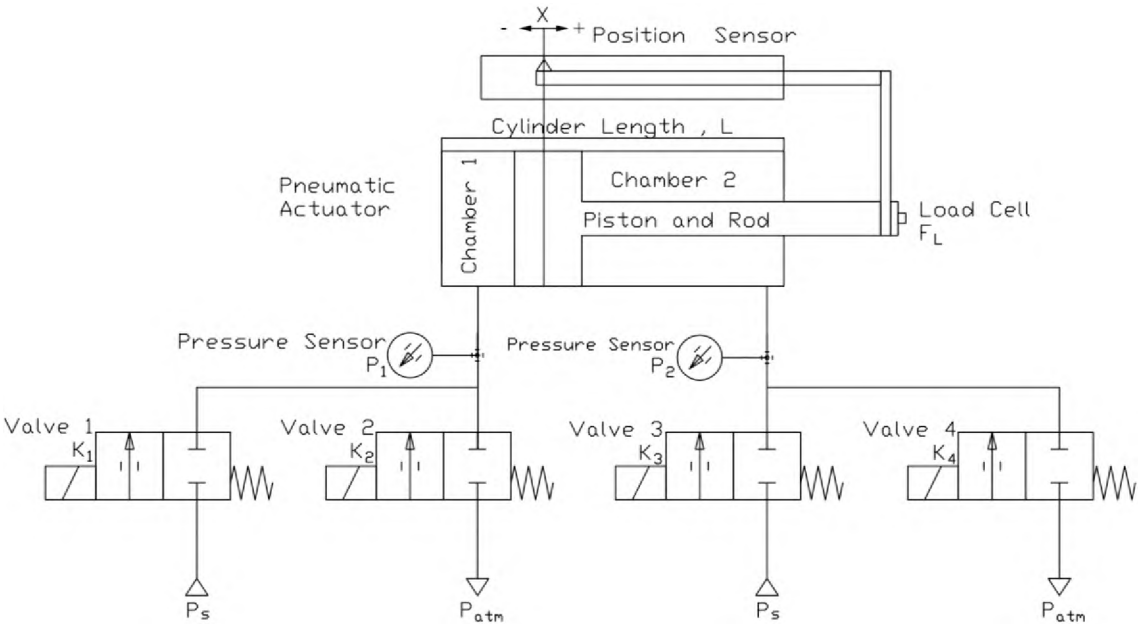

Figure 13: Schematic Diagram of a Pneumatic Actuator

The actuator is comprised of a piston that interacts with the environment, a load cell that measures the force of the actuator on the environment, a potentiometer (position sensor) that measures the position of the actuator, and a cylinder with two chambers whose pressure difference determines the position, force, and compliance of the piston. It should be noted that the position sensor can be either internal or external to the actuator, depending

on chosen system design. It is shown externally in the figure just for clarity. There are also pressure transducers (sensors) near the inlet of each pressure chamber to read the pressure of the chamber. The setup of the valves can differ depending on system design. Four On/Off solenoid valves are employed for this design. Each chamber has a pair of valves that controls the air flow either into or out of the respective chamber. Valves 1 and 3 are connected to the supply pressure, P_s, in order to apply positive pressure, and Valves 2 and 4 are connected to atmospheric pressure, P_{atm}, in order to exhaust air from the chamber. Each valve has two states, either on and allowing air to flow through the valve, or off and blocking air flow. The length of the cylinder is denoted as L and will be used later in this section to find the volume of Chamber 2. This chapter includes the development of a mathematical model that completely describes the pneumatic system through the formation of dynamic model equations for the piston-load, chamber pressures, and valve. The chapter concludes by formulating the control problem and clarifying the control objectives in preparation for the controller design in the next chapter.

A. Piston-Load Dynamics Model

The motion equation for the piston and load interaction is modeled based on Newton's Second Law and the force diagram of the piston, load, and chamber. The force diagram of the forces acting on the piston is shown in Figure 14.

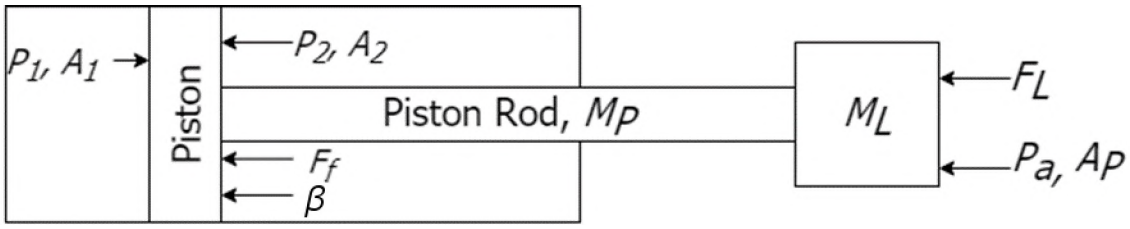

Figure 14: Force Diagram of the Piston and Load

In Figure 14, P_1 and P_2 are the absolute pressures for chambers 1 and 2 respectively. The force of the load is F_L, F_f is the coulomb friction, and β is the viscous friction, which is dependent on velocity. The parameter M_P is the mass of the piston and M_L is the mass of the load. The parameters P_a and A_P are the atmospheric pressure and area of the piston respectively. The area A_P refers to the smaller, rod portion of the piston, while A_1 is the larger disc position of the piston that divides chamber 1 and chamber 2 as it moves, and A_2 is the area of the rod (A_P) subtracted from the area of the disc. Figure 15 shows the cross-section view of the areas explained above. The whole circular area encompassed by the outer circle of radius R_1 is representative of the piston and thus of area A_1, the white area in the center of radius R_P is representative of the piston rod area A_P, and the hatched area between the outer and the inner circles, which is the difference in area between A_1 and A_P, is representative of area A_2.

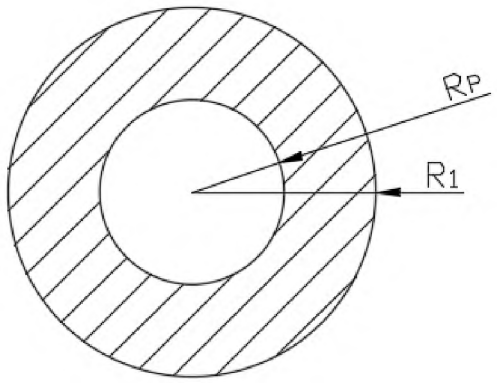

Figure 15: Cross-section of Piston and Rod

According to [2], the resulting dynamics equation based on the above diagram is

$$(M_P + M_L)\ddot{x} + \beta\dot{x} + F_f + F_L = P_1A_1 - P_2A_2 + P_aA_p. \quad (1)$$

On the right side of the equation, P_i multiplied by A_i is equal to force, where i=1 or 2. The right side of (1) is also the input of the system with the areas being known constants and the respective pressures being the input parameters. The piston position input is represented by x. This differential equation will then be solved for acceleration,$\ddot{x}$. This equation fully describes the dynamic motion and interaction of the piston and load.

B. Chamber Pressure Model

The chamber pressure model from [6, 7] describes the pressure within the respective chamber based on the fluid dynamics and energy of the subsystem. The energy equation that describes the system is

$$\dot{Q} + \dot{m}_1\left(h_{enter} + \frac{v_{enter}^2}{2}\right) = \dot{m}_2\left(h_{exit} + \frac{v_{exit}^2}{2}\right) + \dot{E} + \dot{W}. \quad (2)$$

Here it is supposed that the gas is entering chamber 1 and exiting chamber 2. The heat rate for the volume is $\dot{Q}$, the mass flow rate for a given chamber (i=*1,2*) is $\dot{m}_i$, the rate of change of total energy is $\dot{E}$, the work rate delivered to the piston is $\dot{W}$, and h_{enter}, h_{exit}, v_{enter}, *and* v_{exit} represent the enthalpy of the gas and velocity of gas that is either entering or exiting the chamber. Reversing the sign on both of the $\dot{m}_i$ variables will handle the opposite case. This sign reversal will be carried out in later equations for $\dot{m}_i$. This equation is derived from the First Law of Thermodynamics in which the internal energy of a closed system is equal to the difference of the heat and work done by the system on its

surroundings. The following subsections will detail each part of (2) in order to obtain a useful chamber pressure equation based on pressure. The resulting equation will then be used in subsequent sections to describe the control of the system based on the valve position and chamber pressures.

1) Total Energy $\dot{E}$: Again, $\dot{E}$ is the rate of change of total energy in the system. If it is assumed, such as in [7], that the rate of change of the kinetic and potential energies are negligible when compared to the rate of change of the internal energies, then $\dot{E}$ for an adiabatic process for both chambers can be described as

$$\dot{E} = \frac{\partial(U_1)}{\partial t} + \frac{\partial(U_2)}{\partial t} \tag{3}$$

where U_1 and U_2 are the internal energies of each chamber described respectively by

$$U_i = C_v \rho V_i T = \frac{C_v}{R} P_i V_i \tag{4}$$

$$C_v = \frac{R}{k-1}\,. \tag{5}$$

The equation for U_i based on the First Law of Thermodynamics for an ideal gas [6] and the relationship of C_v to R and k, where C_v is the specific heat for a gas at constant volume, R is the individual gas constant defined as $C_P - C_V$, and k is the ratio of specific heat which is defined as $\frac{C_P}{C_V}$. The specific heat for a constant pressure is C_P. Temperature is T, volume of the respective chamber is V_i, and the density is ρ. The resulting equation for U_i is

$$U_i = \frac{1}{k-1} P_i V_i. \tag{6}$$

Differentiating U_i for both P and V, and then substituting back into (3) yields

$$\dot{E} = \frac{1}{k-1}\left[\left(\dot{P}_1 V_1 + P_1 \dot{V}_1\right) + \left(\dot{P}_2 V_2 + P_2 \dot{V}_2\right)\right]. \tag{7}$$

2) Power $\dot{W}$: Power is the rate of change of work, represented in (2) as $\dot{W}$. Work is the multiplication of force and distance. As was mentioned earlier, the force acting in either cylinder is $P_i A_i$, where i=1 or 2. The work W_i for one cylinder is defined by

$$W_i = P_i A_i * D_i = P_i V_i \tag{8}$$

where D_i is the distance from the respective cylinder wall to the disc. Then using the fact that volume is the product of area and distance, (8) then becomes the product of pressure and volume. Assuming the pressure inside the chamber is constant, the derivative of work is then dependent only on the change in volume. Therefore, the final power equation is

$$\dot{W}_i = P_i \dot{V}_i. \tag{9}$$

3) Enthalpy: The enthalpy for the gas entering chamber 1 is expressed as

$$h_{enter} + \frac{v_{enter}^2}{2} = h_0 = C_P T_0. \tag{10}$$

Since the gas that enters this chamber originates in an accumulator, it has zero initial velocity, and therefore is the stagnation point. This can be represented by the stagnation enthalpy, h_0 [7]. This is the enthalpy of the gas held in a supply reservoir that then supplies the system as P_s. Relating this to the stagnation temperature, the stagnation enthalpy can then be represented as a product of the specific heat for the gas at constant pressure, C_P,

and the temperature in the reservoir, T_0. This relates the stagnation enthalpy to the enthalpy of gas entering chamber 1.

Similarly, the enthalpy for the gas exiting chamber two can be represented by

$$h_{exit} + \frac{v_{exit}^2}{2} = h_2 = C_P T_2. \tag{11}$$

Given the assumption that the velocity of the gas exiting chamber 2 is small compared to the one exiting the valve, then (11) relates the enthalpy of chamber 2 to the enthalpy of gas exiting the valve. The entropy of the exiting gas from chamber 2 is h_2 and the temperature of chamber 2 is represented by T_2.

4) Heat Exchange: There are two main thermodynamic processes that can occur based on if heat or substance is exchanged with the system and its surrounding area. The first is the adiabatic process. In this process, energy is only transferred to its surroundings through work and therefore there is no heat exchange. This is described in [16] as either a well-insulated cylinder or that the operation is fast enough that insignificant energy is transferred to the surroundings. In this adiabatic process $Q = 0$. The second process is the isothermal process. In this process, temperature is constant. There is little insulation. The expansion is so slow that there is time for the gas to exchange energy with

the surroundings. It is a common and acceptable assumption to consider the process of gas compression and expansion in a cylinder as adiabatic.

5) Chamber Volume: The volume of each chamber can be described based on the piston's disc position from the left most wall of Figure 13 acting as the origin. The volume and its first derivative are defined as

$$V_1 = A_1 x \tag{12}$$

$$V_2 = A_2(L - x) \tag{13}$$

$$\dot{V}_1 = A_1 \dot{x} \tag{14}$$

$$\dot{V}_2 = -A_2 \dot{x}. \tag{15}$$

6) Resulting Chamber Pressure Equation: When the heat exchange is taken as adiabatic, then (2) becomes

$$\dot{m}_1 \left(h_{enter} + \frac{v_{enter}^2}{2} \right) = \dot{m}_2 \left(h_{exit} + \frac{v_{exit}^2}{2} \right) + \dot{E} + \dot{W}. \tag{16}$$

Next, substituting (5), (7), and enthalpy into (16) yields

$$\dot{m}_1 (C_P T_0) = \dot{m}_2 (C_P T_2) + \frac{C_v}{R} \left(\dot{P}_1 V_1 + P_1 \dot{V}_1 \right) + \frac{C_v}{R} \left(\dot{P}_2 V_2 + P_2 \dot{V}_2 \right) + \dot{W}. \tag{17}$$

Next, (9) is substituted into (17) and the equation is simplified to

$$\dot{m}_1 (C_P T_0) = \dot{m}_2 (C_P T_2) + \frac{C_v}{R} \left(\dot{P}_1 V_1 + \dot{P}_2 V_2 \right) + \left(1 + \frac{C_v}{R} \right) \left(P_1 \dot{V}_1 + P_2 \dot{V}_2 \right). \tag{18}$$

Then, multiplying everything by $\frac{R}{C_P}$ and simplifying yields

$$\dot{m}_1 \left(\frac{R C_P T_0}{C_P} \right) = \dot{m}_2 \left(\frac{R C_P T_2}{C_P} \right) + \frac{R}{C_P} \frac{C_v}{R} \left(\dot{P}_1 V_1 + \dot{P}_2 V_2 \right) + \frac{R}{C_P} \left(1 + \frac{C_v}{R} \right) \left(P_1 \dot{V}_1 + P_2 \dot{V}_2 \right). \tag{19}$$

Since $\frac{R}{C_P}\left(1+\frac{C_v}{R}\right)$ is equal to 1 by using the fact that $R=C_P-C_v$, (19) is the simplified, resulting in

$$\dot{m}_1(RT_0) - \dot{m}_2(RT_2) = \frac{1}{k}\left(\dot{P}_1V_1 + \dot{P}_2V_2\right) + \left(P_1\dot{V}_1 + P_2\dot{V}_2\right). \tag{20}$$

Recall that $\dot{V}_i = A_i\dot{x}$. Lastly, solving for $\dot{P}$, assuming temperature is constant ($T_0 = T_2 = T$), and separating into an equation for each chamber results in

$$\dot{P}_i = \frac{kRT}{V_i}\dot{m}_i - \frac{kP_iA_i}{V_i}\dot{x}. \tag{21}$$

It can be deduced from (21) that for a respective chamber (i = 1,2) that the pressure is the output and is dependent on the mass flow rate, the input, and the piston's position and velocity. The mass flow rate can be further defined in terms of the valve positions as will be discussed in the next section.

C. Valve Model

The valve is what controls the flow of gas into the respective chamber. In this case, there are four valves for the system as seen in Figure 13. There are two valves for each chamber; one to apply positive pressure and the other one for exhausting to atmospheric pressure. The set of valves for each chamber is mutually exclusive, so that air cannot be injected and expelled simultaneously. This means that there are three states that each set can attain; charging (positive pressure on and exhaust off), expelling (positive pressure off and exhaust on), and holding (both off). When a specific valve is off, it does not allow any flow. The mass flow rate for each chamber is

$$\dot{m}_1(K_1, K_2, P_1) = \begin{cases} q_m(P_s, P_1) & for\ K_1 = 1, K_2 = 0 \\ 0 & for\ K_1 = 0, K_2 = 0 \\ -q_m(P_1, P_{atm}) & for\ K_1 = 0, K_2 = 1 \end{cases} \tag{22}$$

$$\dot{m}_2(K_3, K_4, P_2) = \begin{cases} q_m(P_s, P_2) & for\ K_3 = 1, K_4 = 0 \\ 0 & for\ K_3 = 0, K_4 = 0 \\ -q_m(P_2, P_{atm}) & for\ K_3 = 0, K_4 = 1. \end{cases} \tag{23}$$

In (22) and (23) K_i is the on/off state of the respective valve, P_S is supply pressure, P_{atm} is atmospheric pressure, and q_m is defined as

$$q_m(P_{up}, P_{down}) = \begin{cases} C_f A_v C_1 \dfrac{P_{up}}{\sqrt{T}} & if\ \dfrac{P_{down}}{P_{up}} \leq P_{cr} \\ C_f A_v C_2 \dfrac{P_{up}}{\sqrt{T}} \left(\dfrac{P_{down}}{P_{up}}\right)^{\frac{1}{k}} \sqrt{1 - \left(\dfrac{P_{down}}{P_{up}}\right)^{\frac{(k-1)}{k}}} & if\ \dfrac{P_{down}}{P_{up}} > P_{cr}. \end{cases} \tag{24}$$

This equation is the standard expression for the mass flow rate through an orifice of constant area [6] and is a common choice for the modeling of the mass flow rate though the valve openings. In (24), C_f is the discharge coefficient, A_v is the area of the valve orifice (a constant), P_{up} is the upstream pressure, P_{down} is the downstream pressure, and C_1, C_2, and P_{cr} are defined as

$$\begin{aligned} C_1 &= \sqrt{\frac{k}{R}\left(\frac{2}{k+1}\right)^{\frac{k+1}{k-1}}} \\ C_2 &= \sqrt{\frac{2k}{R(k-1)}} \\ P_{cr} &= \left(\frac{2}{k+1}\right)^{\frac{k}{k-1}}. \end{aligned} \tag{25}$$

Equations (22)-(25) mathematically define the flow rate of a fluid through a discrete valve. The input to this system of equations is K_i, the state of each valve. It is the state of these valves that will control the mass flow rate into each chamber.

D. Control problem and objective

Equations (1) and (21)-(25) completely describe the model of the pneumatic system. One objective of the control system is to simultaneously maintain the position and force of the piston at desired values. This task is accomplished through regulating the relationship of force to position in (1). The control of the valves is implemented based on (21) which relates position to pressure. Impedance control must be constructed based on (1) so that piston position and actuator force can be adjusted together. There are two control problems. The first problem is to simultaneously control the relationship of force and position. This is unique in that control solutions typically regulate one type of input. The first problem will be solved by controlling the impedance of the system. The second control problem is to drive the pressure, which is the output of model (21), to follow desired value, despite the presence of high nonlinearity and system uncertainties. The mathematical model for the chamber volume (21) and subsequent valve equations (22)-(25) are nonlinear in nature, which poses complications when it comes to control. This nonlinearity has produced complications in the past for precise position control due to the compressibility of air, the nonlinear flow of air, and friction.

CHAPTER III

CONTROLLER DESIGN

Now that the system model has been described, a controller must be developed to accomplish the control objectives. These objectives are to simultaneously regulate the piston to a desired position and control the force it exerts on the environment if it encounters an object. A block diagram for the control system is depicted in Figure 16.

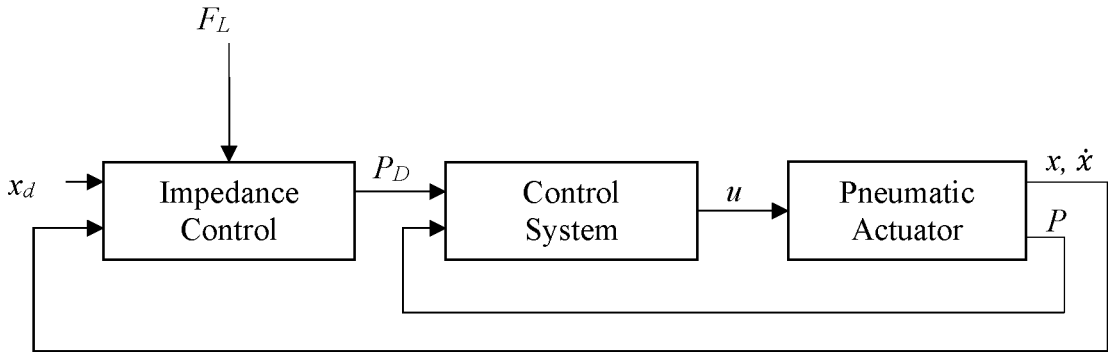

Figure 16: System Block Diagram

This diagram shows the overarching design of the control system. In the diagram, x_d is the desired position chosen by the designer, F_L is the external force that is read by the load cell, P_D is the desired pressure from the impedance control module that will be described below, and u is the control signal for pneumatic actuator. A desired position is inputted into the system. The impedance control block will first calculate the position and

ultimately output a desired pressure. The measured load cell value of the external force at the piston is also added to the impedance module. The error between the desired and the measured pressure is then sent to the controller block, which outputs a control effort. This control effort is a continuous signal but must control discrete valves of a pneumatic actuator.

The remainder of this section is divided as follows. First, the implementation of impedance control will be discussed. Second, the design of the ADRC, ESO-based SMC, and SMC controllers will be described. Lastly, the stability of each controller will be analyzed.

A. Impedance Control

Impedance is defined as the opposition to change. Electrically, impedance is typically defined as voltage divided by current; similarly, mechanical impedance is force divided by velocity. Based on this notion, if force is taken as an output and motion as an input, an impedance equation can be defined to correlate the input to the output. This equation is simply a mass-spring-damper behavior that regulates force to position, velocity, and acceleration.

The dynamics equation of the system is given in (1), which can be reduced to

$$\mathrm{M}\ddot{x} + \beta\dot{x} + F_f + F_L = F_D \tag{26}$$

where the right side of the equation is reduced to a desired force, F_D, and the mass of the piston and load are combined into a generic mass, M. The model for the external force, F_L, is taken from [13] and is mathematically described as

$$\widetilde{M}(\ddot{x} - \ddot{x}_d) + \widetilde{B}(\dot{x} - \dot{x}_d) + \widetilde{K}(\mathrm{x} - x_d) = \mathrm{F}_L. \quad (27)$$

In (27), $\widetilde{M}$, $\widetilde{B}$, and $\widetilde{K}$ are the desired mass, damping, and stiffness coefficients to produce a certain outcome of the system based on the F_L input. The variable x_d is the desired position input of the actuator. Solving (27) for $\ddot{x}$ and then substituting it into (26) yields

$$\frac{M}{\widetilde{M}}\left(F_L - \widetilde{B}(\dot{x} - \dot{x}_d) - \widetilde{K}(\mathrm{x} - x_d)) + \widetilde{M}\ddot{x}_d\right) + \beta\dot{x} + F_f + F_L = F_D. \quad (28)$$

Impedance control module is represented by (28) which relates force with position. The module provides a desired force output. However, the desired force needs to be converted into a desired pressure for each chamber. Two additional equations are needed to convert this desired force into a desired pressure for two chambers. The two equations are

$$F_D = P_{1D}A_1 - P_{2D}A_2 - P_{atm}A_P \quad (29)$$

$$P_{sum} = P_{1D} + P_{2D}. \quad (30)$$

In (29) and (30), P_{1D} and P_{2D} are the desired pressures of chamber 1 and 2 respectively. The sum of pressures, P_{sum}, is a chosen parameter of the total pressure that will be supplied to the system. The total force F_D, or desired force in this case, is equal to the resultant of all the pressures acting on the system. The desired force F_D can be obtained from (28). The atmospheric pressure P_{atm} is known. The only two unknowns among (29) and (30) are the desired chamber pressures, which can then be solved for through substitution. This set of equations allows the impedance module to output a useful vector of desired pressures that will then be used by the controller design in the next section.

B. Active Disturbance Rejection Control

1) Controller: Active Disturbance Rejection Control was first proposed in [32] in a nonlinear form, and then linearized in [33]. The linearized ADRC has wide applications such as in [34-37]. It consists of a feedback controller and an extended state observer (ESO). The ESO estimates and compensates both internal and external disturbances without the need for an accurate mathematical model. A generalized disturbance is defined as the combination of the unknown system dynamics, as well as the external disturbances, and is compensated by the feedback controller. The block diagram for a first order ADRC structure is depicted in Figure 17.

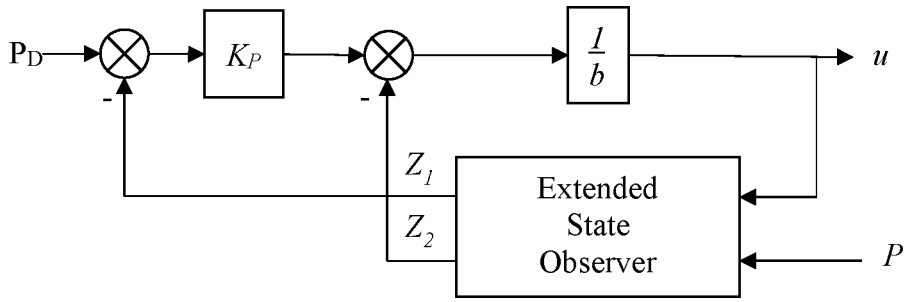

Figure 17: ADRC Block Diagram

The major component of ADRC is the ESO to estimate the system states and disturbances. An extended state in ESO is utilized to approximate the generalized disturbance. Another major component of first order ADRC is a proportional controller to control the plant. It is the use of the ESO to cancel the nonlinear disturbances that allows for the use of straightforward proportional control. In order to implement the ADRC, the system to be controlled must be of the form:

$$y^{(r)}(t) = bu(t) + f\big(y(t), u(t), d(t)\big). \tag{31}$$

In (31), *y* is a generic output and dependent on time, *t*. In addition, *b* is a controller gain, *u(t)* is a generic time dependent input, and *f(y(t), u(t), d(t))*, represented as $f(\cdot)$ for simplicity, is the generalized disturbance that is dependent on the input, output, and a disturbance, *d(t)*. According to [34], for a given transfer function *G(s)* where *m* is the highest degree of the numerator and *n* is the highest degree of the denominator, then the order of the system, *r*, in (26) is

$$r = n - m. \tag{32}$$

This *r* is also equal to the highest order derivative for the system. Using (31) as a template, the pneumatic actuator plant given by (21) can be related to (31) where $b = \frac{kRT}{V_i}$, $u = \dot{m}_i$, $f(\cdot) = -\frac{kP_iA}{V_i}\dot{x}$, and $y = P_i$. An estimate of *b*, defined as $\hat{b}_{ADRC}$ for this controller, will be chosen as a constant in the model.

As described above, the control effort from the controller is the mass flow rate. Analyzing the mass flow rate equations (22) and (23), we can see that if the positive pressure valve (U_1 for chamber 1 and U_3 for chamber 2) is on, then the mass flow rate is positive. If the exhaust valve (U_2 for chamber 1 and U_4 for chamber 2) is on, then the mass flow rate is negative. Lastly, if both valves are off for a chamber, then the mass flow rate is zero. Thus, the direction of the mass flow rate for the given chamber can be directly linked to the excitation of its discrete valves.

The state space representation can now be developed. The state variables are chosen based on $x_n = P_i^{(n-1)}$ for *n = 1 to r*, $x_{r+1} = f(\cdot)$, and $h = \dot{f}(\cdot)$ [34]. For the first order

system of (21), this leads to the definition of $x_1 = P_i$.and $x_2 = f(\cdot)$.The state space model can then be defined as

$$\begin{cases} \dot{X} = AX + Bu + Eh \\ y = CX, \end{cases} \tag{33}$$

where $X = \begin{bmatrix} x_1 \\ x_2 \end{bmatrix}$, $A = \begin{bmatrix} 0 & 1 \\ 0 & 0 \end{bmatrix}$, $B = \begin{bmatrix} \hat{b}_{ADRC} \\ 0 \end{bmatrix}$, $C = [1 \quad 0]$, and $E = \begin{bmatrix} 0 \\ 1 \end{bmatrix}$. Since $f(\cdot)$, the generalized disturbance, cannot be measured, an ESO must be developed to estimate it The ESO is represented by

$$\begin{cases} \dot{Z} = AZ + Bu + L(y - \hat{y}) \\ \hat{y} = CZ, \end{cases} \tag{34}$$

where $Z = \begin{bmatrix} z_1 \\ z_2 \end{bmatrix}$ which is a state vector of ESO, is approximately equal to X such that $z_1 \approx P$ and $z_2 \approx f(\cdot)$. The observer gain vector L is defined as $L = \begin{bmatrix} l_1 \\ l_2 \end{bmatrix}$and is selected such that the characteristic equation of the observer will be $(s + \omega_o)^{r+1}$ in which ω_o is defined as the positive observer bandwidth. Thus, using the equation given in [34], each observer gain is defined as

$$l_i = \frac{(r+1)!}{i!\,(r+1-i)!}\omega_o^i, i = 1, \ldots, r+1. \tag{35}$$

The observer gain vector then becomes $L = \begin{bmatrix} 2\omega_o \\ {\omega_o}^2 \end{bmatrix}$.

From [33], the control law for the system with ESO is defined as

$$u_{ADRC} = \frac{(-z_2 + u_0)}{\hat{b}_{ADRC}} \tag{36}$$

where u_{ADRC} is the control signal for the ADRC controller. Substituting (36) into (31), and assuming z_2 accurately estimates $f(\cdot)$ and $\hat{b}_{ADRC}$ accurately estimates b, yields

$$\dot{P}_i = \frac{b(-z_2 + u_0)}{\hat{b}_{ADRC}} + f(\cdot) \approx u_0. \tag{37}$$

Equation (37) then shows that successful tracking of the system and good estimation of b reduces the output to a simple and controllable u_0. The variable u_0 can be defined based on the control goal for the system. For this system, that control goal is to drive the pressure to a desired value. This can be simply controlled by a state feedback controller defined as

$$u_0 = k_p(P_D - z_1), \tag{38}$$

where P_D is the desired pressure and k_p is the proportional gain. The tuning is simplified in [33] by defining $k_p = \omega_c$, where the controller bandwidth is represented by ω_c.

The linear ESO is defined as (34) and the linear ARDC (LARDC) is defined as (38). This equation development further shows that the tuning of the ADRC is only dependent on the controller and observer gains, ω_c and ω_o respectively; thus, making this solution easy to implement and tune. To restate, ADRC does not need an accurate model of the system. It uses the ESO to estimate the disturbances and uncertainties so that the plant can be controlled by a proportional controller as shown in (38). The powerfulness in this control solution is that the exact model and parameters do not need to be found for the system to be accurately controlled. The nonlinearity of the air flow and the uncertainties in the exact numeric values of the thermodynamic equations thus can be compensated for by the ADRC control approach.

The estimation of b, $\hat{b}_{ADRC}$, is actually taken from the estimation for b that is developed for SMC in [35]. For a b that is unknown but has known bounds the geometric mean of these bounds can be found. First, the maximum and minimum values are found using

$$b_{max} = \frac{kRT}{A_i x_{inact}} \tag{39}$$

$$b_{min} = \frac{kRT}{A_i L}, \tag{40}$$

where A_i is the area of a given chamber with $i=1,2$, x_{inact} is a small distance between the end of the chamber and the separating disc that is still present when the chamber is fully collapsed. The distance is a very small gap that is necessary to allow air to move the disc again when necessary. The estimation of b was initially defined as the geometric mean of the maximum and minimum values:

$$\hat{b}_{ADRC} = \sqrt{b_{min} b_{max}}. \tag{41}$$

However, through empirical testing, it was found that estimating b when the chamber was a full length produced a better result. Therefore, b is estimated as

$$\hat{b}_{ADRC} = b_{min}. \tag{42}$$

2) ADRC Stability: ADRC stability is based on the proof developed for a general n-th order system in [36]. In this section, the convergence of estimation error for

ESO is proved. In addition, the stability of ADRC controlled closed-loop system is demonstrated.

a) Extended State Observed Error Dynamics: As stated above in (34), the plant dynamics of the ESO are

$$\begin{aligned} \dot{Z} &= AZ + Bu + L(y - \hat{y}) \\ \hat{y} &= CZ. \end{aligned} \tag{34}$$

Then, letting the estimation error between actual and estimated states be defined as

$$\tilde{e} = X - Z = \begin{bmatrix} \tilde{e}_1 \\ \tilde{e}_2 \end{bmatrix} \tag{43}$$

where

$$\tilde{e}_1 = P - z_1 \tag{44}$$

$$\tilde{e}_2 = f(\cdot) - z_2. \tag{45}$$

The error vector, e, is defined as

$$e = \begin{bmatrix} e_1 \\ e_2 \end{bmatrix} = \begin{bmatrix} P - P_D \\ \dot{P} - \dot{P}_D \end{bmatrix} \tag{46}$$

where $\dot{P}_D$ is zero since the desired pressure is constant. Recalling the state equations to be

$$\begin{cases} \dot{X} = AX + Bu + Eh \\ y = CX, \end{cases} \tag{33}$$

Differentiating (43), the error dynamics of the ESO then become,

$$\dot{\tilde{e}} = (A - LC)\tilde{e} + Eh \tag{47}$$

Next, a state transformation can be defined as

$$\tilde{e} = \Lambda\xi \tag{48}$$

Where Λ and ξ are defined as

$$\Lambda = \begin{bmatrix} {\omega_o}^{-1} & 0 \\ 0 & 1 \end{bmatrix}$$
$$\xi = \begin{bmatrix} \xi_1 \\ \xi_2 \end{bmatrix}. \tag{49}$$

Substituting (48) into (47) results in

$$\Lambda\dot{\xi} = (A - LC)\Lambda\xi + Eh. \tag{50}$$

Simplifying (50), the error dynamics can then be rewritten as

$$\epsilon\dot{\xi} = A_z\xi + \epsilon Eh \tag{51}$$

where ϵ and A_z are defined as

$$\epsilon = \frac{1}{\omega_o}$$
$$A_z = \begin{bmatrix} -2 & 1 \\ -1 & 0 \end{bmatrix}. \tag{52}$$

The eigenvalues of matrix A_z are

$$\lambda_i\{A_z\} = -1 \; \forall \; i = 1,2. \tag{53}$$

As stated in [36], this means that matrix A_z is Hurwitz and invertible with the observer bandwidth ω_o as the tuning parameter.

b) Feedback Loop Error Dynamics: The control law for ADRC from the Controller Design section is restated as

$$u = \frac{-z_2 + u_0}{\hat{b}_{ADRC}} \tag{36}$$

where

$$u_0 = k_P(P_D - z_1). \tag{38}$$

To obtain the error dynamics, the tracking error is defined as

$$e = P - P_D \tag{54}$$

$$\dot{e} = A_e e + B_e u + B_f f(\cdot) \tag{55}$$

where P_D is a time-varying function from the impedance controller. For this specific control system,

$$\begin{aligned} A_e &= 0 \\ B_e &= b \\ B_f &= 1. \end{aligned} \tag{56}$$

The control law, u, can then be re-defined as

$$u = \frac{-z_2 + k_p(-e_1 + \tilde{e}_1)}{\hat{b}_{ADRC}} \tag{57}$$

where

$$z_2 = f(\cdot) - \tilde{e}_2. \tag{58}$$

The control law can then be simplified to

$$u = \frac{-f(\cdot) + K_f \tilde{e} - Ke}{\hat{b}_{ADRC}} \tag{59}$$

where K_f and K are defined as

$$\begin{aligned} K_f &= [k_p \quad 1] \\ K &= k_p. \end{aligned} \tag{60}$$

Substituting (59) into (55) and assuming $\hat{b}_{ADRC}$ accurately estimates b yields

$$\dot{e} = A_e e + K_f \tilde{e} - Ke - f(\cdot) + B_f f(\cdot) \tag{61}$$

Define $A_f = A_e - K$. Using the state transformation in (48) and (49), we can rewrite (56) as

$$\dot{e} = A_f e + K_f \Lambda \xi \tag{62}$$

where A_f is defined as

$$A_f = -k_p = -\omega_c. \tag{63}$$

The eigenvalue of A_f is equal to -ω_c which is less than zero since ω_c is a strictly positive value which makes the matrix Hurwitz. By the Lyapunov stability theory, since both the error dynamics of the ESO and feedback loop are stable, thus the controller is stable.

C. *Sliding Mode Control*

Sliding Mode Control (SMC) is a nonlinear control method that is developed based on the Lyapunov function. Since it uses a Lyapunov function as part of the control design, the stability of the controller is proven as part of the design process. The plant model (21) is repeated here:

$$\dot{P}_i(t)(t) = \frac{kRT}{V_i}\dot{m}_i - \frac{kP_iA_i}{V_i}\dot{x} \tag{21}$$

where we define $b = \frac{kRT}{V_i}$, $u_{SMC} = \dot{m}_i$, $f(\cdot) = -\frac{kP_iA_i}{V_i}\dot{x}$, and $y = P_i$. This has been developed from the general first order system equation in (31). For the SMC controller, b will be denoted as b_{SMC} to differentiate it from the other controllers. The value of b_{SMC} will be calculated in real time for SMC, unlike the estimated value in ADRC.

From [35], the sliding surface and its derivative can be defined as

$$s_i = e_i \tag{64}$$

$$\dot{s}_i = \dot{e}_i = \dot{P}_i - \dot{P}_{D_i} = f(\cdot) + b_{SMC}u_{SMC} \tag{65}$$

where $\dot{P}_{D_i}$ is equal to zero since the desired pressure should be constant and e_i, the error between the actual pressure and the desired pressure for a given chamber, is defined as

$$e_i = P_i - P_{D_i} \tag{66}$$

where P_i is the actual pressure of a given chamber that is provided to the system via a sensor and P_{D_i} is the desired pressure for a given chamber from the impedance module that is ideally a constant. For simplicity, the subscript *i* is disregarded with the assumption that each equation can be developed for either chamber 1 or chamber 2.

Then, the Lyapunov function is chosen to be

$$V = \frac{1}{2}s^2 \tag{67}$$

$$\dot{V} = s\dot{s}. \tag{68}$$

Substituting (65) into (68) yields

$$\dot{V} = s(f(\cdot) + b_{SMC}u_{SMC}). \tag{69}$$

The control effort, u_{SMC}, is defined as

$$u_{SMC} = \frac{\hat{u}_{SMC} - k_{SMC}sgn(s)}{b_{SMC}} \tag{70}$$

where $\hat{u}_{SMC}$ is an estimate of the equivalent control and added to this is a discontinuous term across the surface to satisfy the sliding condition. The sign function (*sgn*) is defined as

$$sgn(s) = \begin{cases} 1 & if\ s > 0 \\ 0 & if\ s = 0. \\ -1 & if\ s < 0 \end{cases} \tag{71}$$

The goal of SMC is to pick a well-behaved function of tracking error, and then select a control law such that the derivative of the Lyapunov function (based on s^2) is negative definite despite the presence of model imprecision and disturbances as described in

[35].This function of tracking error is sliding surface *s*. The problem of tracking a reference signal is then reduced to that of keeping the scalar quantity *s* at zero. Substituting (70) into (65) yields

$$\dot{s} = f(\cdot) + b_{SMC}\frac{\hat{u}_{SMC} - k_{SMC}sgn(s)}{b_{SMC}}. \tag{72}$$

From (72), we choose $\hat{u}_{SMC} = -\hat{f}(\cdot)$ where $\hat{f}(\cdot)$ is an estimate of the dynamics and is defined as

$$\hat{f}(\cdot) = -\frac{kP_iA_i\dot{x}}{V_i}. \tag{73}$$

An estimate of $P_i$is defined as the average of the maximum and minimum pressure possible in the system and is represented as P_{avg}. Since the volume, V, of the chamber can be expressed as $V_i=A_ix$ then (73) becomes

$$\hat{f}(\cdot) = -k\frac{(P_{atm} + P_{sum})}{2}\frac{\dot{x}}{x} = -kP_{avg}\frac{\dot{x}}{x}. \tag{74}$$

This leaves the control law now equal to

$$u_{SMC} = \frac{-\hat{f}(\cdot) - k_{SMC}sgn(s)}{b_{SMC}}. \tag{75}$$

For the controller to be stable, $\dot{V}$ must be less than or equal to zero. Substituting (75) into (69) and rearranging yields

$$\dot{V} = s\big(f(\cdot) - \hat{f}(\cdot)\big) - sk_{SMC}sgn(s). \tag{76}$$

The estimation error on $f(\cdot)$ is assumed to be bounded by some known function

$$F(\cdot) \geq \left|f(\cdot) - \hat{f}(\cdot)\right|. \tag{77}$$

This bounded function, *F(x)*, is found by first substituting the values of $f(\cdot)$ and $\hat{f}(\cdot)$ into (77), yielding

$$F(\cdot) \geq \left| -\frac{kP\dot{x}}{x} - \frac{-kP_{avg}\dot{x}}{x} \right|. \tag{78}$$

Since *k* and *x* are always positive by definition, (36) then becomes

$$F(\cdot) \geq \frac{k}{x}\left|(-P + P_{avg})\dot{x}\right|. \tag{79}$$

Since pressure is always a positive value, the quantity $(P\text{-}P_{avg})$ will always be less than P_{avg}. Thus, to make $F(\cdot)$ always greater than the right side of the equation, it can be set to the same value as $\hat{f}(\cdot)$ with the addition of taking the absolute value of the velocity, $\dot{x}$, since that can produce a negative value. This makes $F(\cdot)$ equal to

$$F(x) = k\frac{(P_{atm} + P_{sum})}{2}\frac{|\dot{x}|}{x} = kP_{avg}\frac{|\dot{x}|}{x}. \tag{80}$$

Now, substituting (77) into (76) and simplifying yields

$$\dot{V} \leq s(F(x)) - k_{SMC}|s|. \tag{81}$$

For this to be true and the system to be stable, *k* is set equal to $F(x)+\eta$. This simplifies (81) to

$$\dot{V} \leq -\eta_{SMC}|s| \tag{82}$$

where η_{SMC} is a chosen strictly positive constant. Substituting this into the control effort yields

$$u_{SMC} = \frac{-\hat{f}(\cdot) - (F(\cdot) + \eta_{SMC})sgn(s)}{b_{SMC}} \tag{83}$$

which is a stable controller based on the Lyapunov stability method.

Additionally, the sign function was replaced by a saturation function to improve performance by smoothing out the control discontinuity in a thin boundary layer (i.e. chattering effects). This function is defined as

$$sat(\frac{s}{\Phi}) \tag{84}$$

where Φ is the thickness of the boundary layer. The saturation function work in the following way:

$$sat(s) = \begin{cases} \frac{s}{\Phi} & if\ |s| \leq \Phi \\ sgn(s) & else \end{cases}. \tag{85}$$

From a practical point of view in (64), as Φ gets smaller the function acts closer to a sign function. The s/Φ portion of the equation is basically finding a percentage of Φ in comparison to s, which is the error between the actual and desired pressure. So, Φ can be chosen to produce tracking within a guaranteed precision based on

$$\varepsilon = \frac{\Phi}{\lambda^{n-1}} \tag{86}$$

where ε is the boundary layer width. Since n in (65) is equal to 1 in a first order system, then ε reduces to just Φ. So Φ becomes a chosen parameter for desired tracking precision. The control law then, finally, becomes

$$u = \frac{-\hat{f}(\cdot) - (F(\cdot) + \eta_{SMC})sat(\frac{s}{\Phi})}{b_{SMC}}. \tag{87}$$

D. Extended State Observer-based SMC

The design of the ESO-based SMC is based on the same first-order system as was defined in (21) :

$$\dot{P}_i(t) = \frac{kRT}{V_i}\dot{m}_i - \frac{kP_iA_i}{V_i}\dot{x} = bu + f(\cdot) \tag{21}$$

where we let $b = \frac{kRT}{V_i}$, $u = \dot{m}_i$, $f(\cdot) = -\frac{kP_iA}{V_i}\dot{x}$, and $y = P_i$. An estimate of b, defined as $\hat{b}_{ESMC}$ for this controller, will be chosen as a constant in the model. Again, the subscript *i* is disregarded for simplicity, but under the assumption that these equations can be applied to either chamber.

The addition of the ESO is the major difference between the previously mentioned SMC controller and this current approach. Adding the ESO will eliminate the need for real-time computation of variables and allow instead for the total disturbance to be estimated, without a reduction in performance. The ESO model is the same as the one used for ADRC. Reproducing for clarity, the state space model is defined as,

$$\begin{cases} \dot{Z} = AZ + Bu + L(y - \hat{y}) \\ \hat{y} = CZ, \end{cases} \tag{34}$$

where $Z = \begin{bmatrix} z_1 \\ z_2 \end{bmatrix}$ and *Z*, an estimation of the states from the ESO, is approximately equal to *X* such that $z_1 \approx P$ and $z_2 \approx f(\cdot)$. The observer gain vector *L* is defined as $L = \begin{bmatrix} l_1 \\ l_2 \end{bmatrix}$ and is selected such that the characteristic equation of the observer will be $(s + \omega_o)^{r+1}$ in which ω_o is defined as the positive observer bandwidth. Thus, using the equation given in [34], observer gain vector is defined as $L = \begin{bmatrix} 2\omega_o \\ {\omega_o}^2 \end{bmatrix}$.

Adding this ESO to the SMC eliminates the need for the controller to use the position and velocity feedback from the system that were required to find the values of *F(x)* and $\hat{f}$. Removing these inputs makes the controller more realistic in actual practice. While these inputs may be measurable in most cases, they can still be prone to errors and

bandwidth issues. So, while the controller complexity is increased with the addition of ESO, it creates a system that is realistic in practice. For the same reason of not needing the position and velocity feedback from the system, b is also an estimated constant in this controller, defined here as $\hat{b}_{ESMC}$. The same estimate for $\hat{b}_{ESMC}$ is used as was developed for $\hat{b}_{ADRC}$ in (89).

The SMC portion of this controller is developed just as above using the approach in [35] where the sliding surface, s, is defined relative to the order of the system. For a first-order system such as this, s and its derivative are defined as

$$s = e = P - P_d \tag{88}$$

$$\dot{s} = \dot{e} = \dot{P} - \dot{P}_d = \dot{P} \tag{89}$$

where the derivative of desired pressure is zero for all cases since it is a constant. The variable e is again the error between the actual and desired pressure. Then, (21) can be substituted into (89). The goal is again to create a control law, u, that cancels the system dynamics f and b, leaving a simplified proportional controller. For this controller an approach like [36] is used by employing the constant plus proportional reaching law developed in [37]. This reaching law is used to increase the reaching rate of the controller. The discontinuous control law is defined as

$$-P_{ESMC}\hat{s} - \eta_{ESMC} sgn(\hat{s}) \tag{90}$$

where P_{ESMC} and η_{ESMC} are positive gain terms. Combining the discontinuous control law with the continuous control law, the control effort can now be defined as

$$u_{ESMC} = \frac{\hat{u} - P_{ESMC}\hat{s} - \eta_{ESMC} sgn(\hat{s})}{\hat{b}_{ESMC}}. \tag{91}$$

where $\hat{u}$ is the continuous control law, and $\hat{s}$ is defined as

$$\hat{s} = z_1 - P_d. \tag{92}$$

The continuous control law, $\hat{u}$, will be defined as in SMC control as $\hat{f}(\cdot)$. However, this will end up being estimated by the ESO. Using only the constant reaching law in (82) was not sufficient in producing the desired outcome of the controller. So, employing the reaching law approach discussed in [37], a constant plus proportional reaching law was then used so that the dynamics of the switching function could be manipulated, and the reaching rate increased. Adding this approach to the control strategy produced satisfactory results. The control law then becomes

$$u_{ESMC} = \frac{-\hat{f}(\cdot) - P_{ESMC}\hat{s} - \eta_{ESMC}sgn(\hat{s})}{\hat{b}_{ESMC}}. \tag{93}$$

The ESO-based SMC is based on the chosen Lyapunov function as was defined in (67) and (68) is reproduced here:

$$V = \frac{1}{2}s^2 \tag{67}$$

$$\dot{V} = s\dot{s}. \tag{68}$$

where s is sliding surface as defined in (88) . The term $\tilde{s}$ is defined as the difference between the estimated and actual sliding surface:

$$\tilde{s} = s - \hat{s}. \tag{94}$$

Then, following the process in [38], substituting (89) into (68) results in

$$\dot{V} = s\dot{P}. \tag{95}$$

Next, assuming $\hat{b}_{ESMC}$ is a good estimate of b, substituting (93) into (21) yields

$$\dot{P} = f(\cdot) - P_{ESMC}\hat{s} - \eta_{ESMC}sgn(\hat{s}) - \hat{\hat{f}}(\cdot). \tag{96}$$

By then substituting (96) into (95) yields

$$\dot{V} = s\big(f(\cdot) - P_{ESMC}\hat{s} - \eta_{ESMC}sgn(\hat{s}) - \hat{f}(\cdot)\big). \tag{97}$$

Using F in (53), we can simplify (73) as

$$\begin{aligned} \dot{V} = & -P_{ESMC}\hat{s}s - \eta_{ESMC}ssgn(\hat{s}) + s\big(f(\cdot) - \hat{f}(\cdot)\big) \\ & = -P_{ESMC}\hat{s}s - \eta_{ESMC}|s| + Fs. \end{aligned} \tag{98}$$

Then, using $\tilde{s}$ as defined in (94), (98) becomes

$$\dot{V} = -P_{ESMC}(-\tilde{s} + s)s - \eta_{ESMC}|s| + Fs. \tag{99}$$

Finally, simplifying (99), results in

$$\dot{V} = -P_{ESMC}s^2 - \eta_{ESMC}|s| + s(F + P_{ESMC}\tilde{s}). \tag{100}$$

For the controller to be stable, $\dot{V}$ must be strictly less than zero. Thus, for (100) to produce a stable controller the following must be true:

$$P_{ESMC}s^2 + \eta_{ESMC}|s| - P_{SMC}\tilde{s}s \; > Fs. \tag{101}$$

Finally, substituting the ESO estimates into (91) produces the control law

$$u_{ESMC} = \frac{-z_2 - P_{ESMC}(z_1 - P_D) - \eta_{ESMC}sgn(z_1 - P_D)}{\hat{b}_{ESMC}}. \tag{102}$$

CHAPTER IV

SIMULATION

In this chapter, MATLAB/Simulink is used to simulate the impedance control of the pneumatic system using the ADRC, SMC, and ESO-based SMC control techniques. The ADRC controller contains a proportional controller with ESO feedback. The SMC controller is based on known system states without any observer. Finally, the ESO-based SMC controller is like the SMC controller except that it uses an ESO to estimate pressure and disturbance. It also contains an estimate for the control gain. The building of the simulation is described in Section A. Section 0 presents the results of the three different designs. Finally, Section Coffers discussion on the results.

A. Simulation Design

The equations for the pneumatic actuator system and the controller that were detailed in previous chapters are used to create the Simulink model. Recall in Figure 16 a general diagram of how the system is designed. The impedance control module and the pneumatic actuator module are constructed in Simulink and remain the same for different controller designs. Different controller produces different control effort for pressure control.

One other component added to the system, in order to demostrate impedance control when the actuator comes into contact with an object, is a stiff-spring system to model a wall or other stiff object that will apply an equal and opposite force to the piston. The external force, F_L, is modeled using the following equation.

$$\begin{cases} F_L = k_{obj} * x & if\ x > x_{obj} \\ F_L = 0 & otherwise \end{cases} \tag{103}$$

In (103), x is the current position of the actuator, k_{obj} is the chosen stiffness of the object, and x_{obj} is the position of the object that the actuator will contact.

The Simulink model for impedance control is a two step process as diagramed in Figure 18. First, (28) is used to convert desired position, current position and velocity, and piston force into a desired force. Then, (29) and (30) are used to determine desired pressures for both chambers based on the desired force. This desired pressure is then used by the control system to regulate the actual pressure to the time-varying P_D.

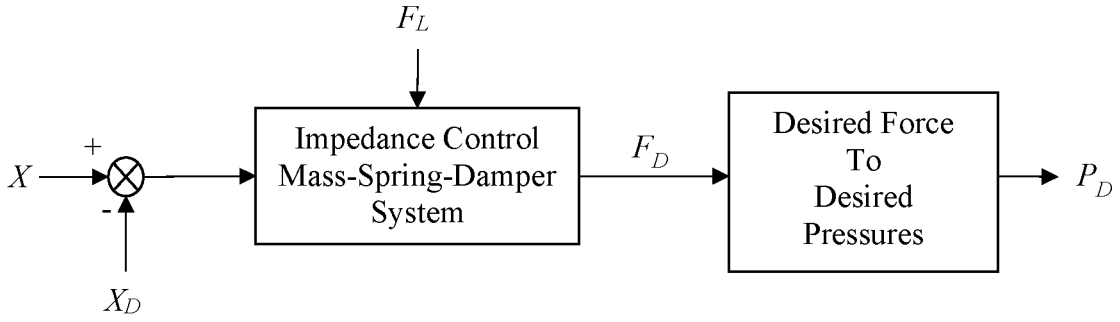

Figure 18: Impedance Control

The Pneumatic Actuator system uses the incoming control effort from the controller to determine the states of the valves for the specific chamber. Then, the valve state is equated to mass flow rate through (22) and (23). Since the mass flow rate in (22) has its

positive, negative, or zero value based on the state of the valves, this can be used conversely in that if the mass flow rate is positive, then positive pressure is applied, if the mass flow rate is negative then exhaust is applied, and if it is zero then both valves are off. Mass flow rate is then equated to pressure by (21). Lastly, through (1), the pressure of each chamber is used to determine the position of the rod.

The ADRC, ESO-based SMC, and SMC block diagrams are shown in Figure 19 - Figure 21. These are the block diagrams of the mathematical equations developed in the previous section that are used to create the actual Simulink models. The actual Simulink models are provided in the Appendix.

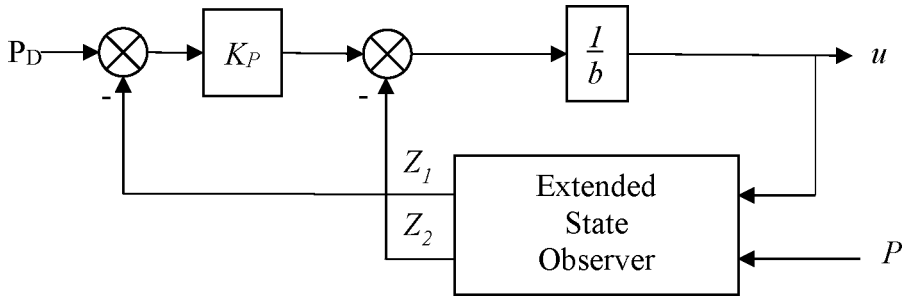

Figure 19: ADRC Block Diagram

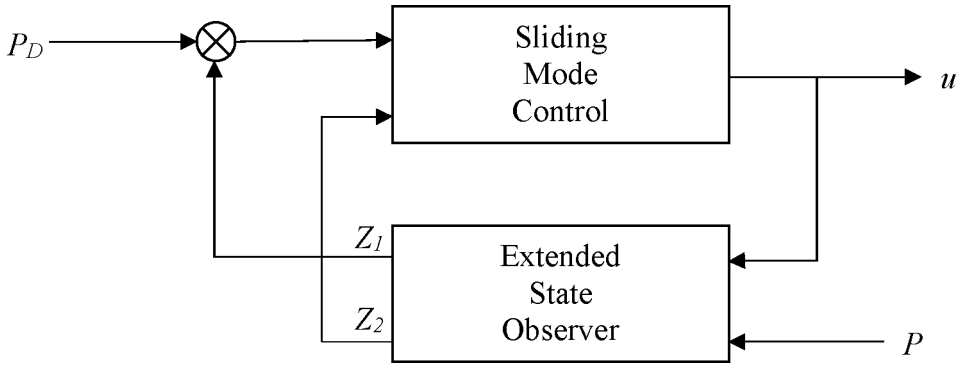

Figure 20: ESO-based SMC Diagram

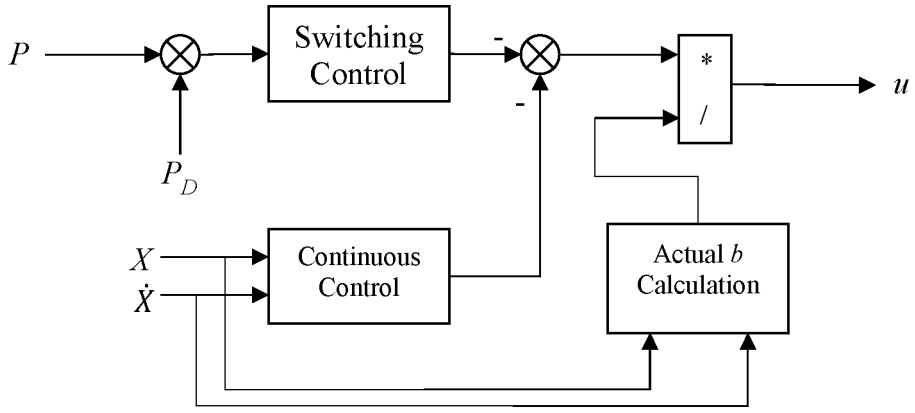

Figure 21: SMC Diagram

The parameters used to complete the simulations are listed in

Table I and Table II.

Table I: System Parameters

Parameter	Value	Unit of Measurement
$\widetilde{K}$	6.25×10^4	*N/m*
$\widetilde{M}$	0.1	*kg*
$\widetilde{B}$	500	*N/m/s*
M	0.1	*Kg*
β	50	*Ns/m*
P_{atm}	101352 (14.7)	*Pa (PSI)*
P_{sum}	758423 (110)	*Pa (PSI)*
d_1	0.020	*m*
d_p	0.008	*m*
k	1.4	Nondimensional
R	287	*J/mol/K*
T	294	*K*
C_f	0.25	Nondimensional
A_v	0.005	*m*
L	0.150	*m*
X_{inact}	1×10^{-4}	*M*
k_{obj}	2.5×10^6	*N*
x_{obj}	0.08	*m*

Table II: Controller Parameters

Parameter	Value	Unit of Measure
η_{SMC}	1×10^{12}	Nondimensional
Φ	7×10^6	Nondimensional
ω_c (ADRC)	5×10^4	Nondimensional
ω_o (ADRC)	$5\ \omega_c$	Nondimensional
ω_c (ESO-based SMC)	3×10^2	Nondimensional
ω_o (ESO-based SMC)	$5\ \omega_c$	Nondimensional
$\widehat{b}_{ESMC}$	2.5×10^9	$J/mol/m^3$
η_{ESMC}	1×10^{-5}	Nondimensional
P_{ESMC}	1×10^5	Nondimensional

B. Simulation Results

The design detailed in the previous subsection was simulated and the following key elements of the system were recorded. The elements of piston position, control effort, chamber pressure, piston force regulation, control valve state, and ESO estimation play key roles in determining the success of the controller. The mass-spring-damper system designed with the chosen parameters used in the impedance control module has a settling time of 0.0184 seconds. This system must be critically damped to function properly. While a non-critically damped system would function, it could produce undesirable fluctuations in the position control of the system.

1) Position: A key goal of this design is for the piston of the pneumatic actuator to be commanded to any position within its range of motion. Figure 22(a) shows the resulting piston position outputs (x) of all three controllers, comparing the commanded positions to the simulated positions of all three systems. A detailed view of the position is

shown in Figure 22(b) where three controllers drive the rod of the actuator to the command position.

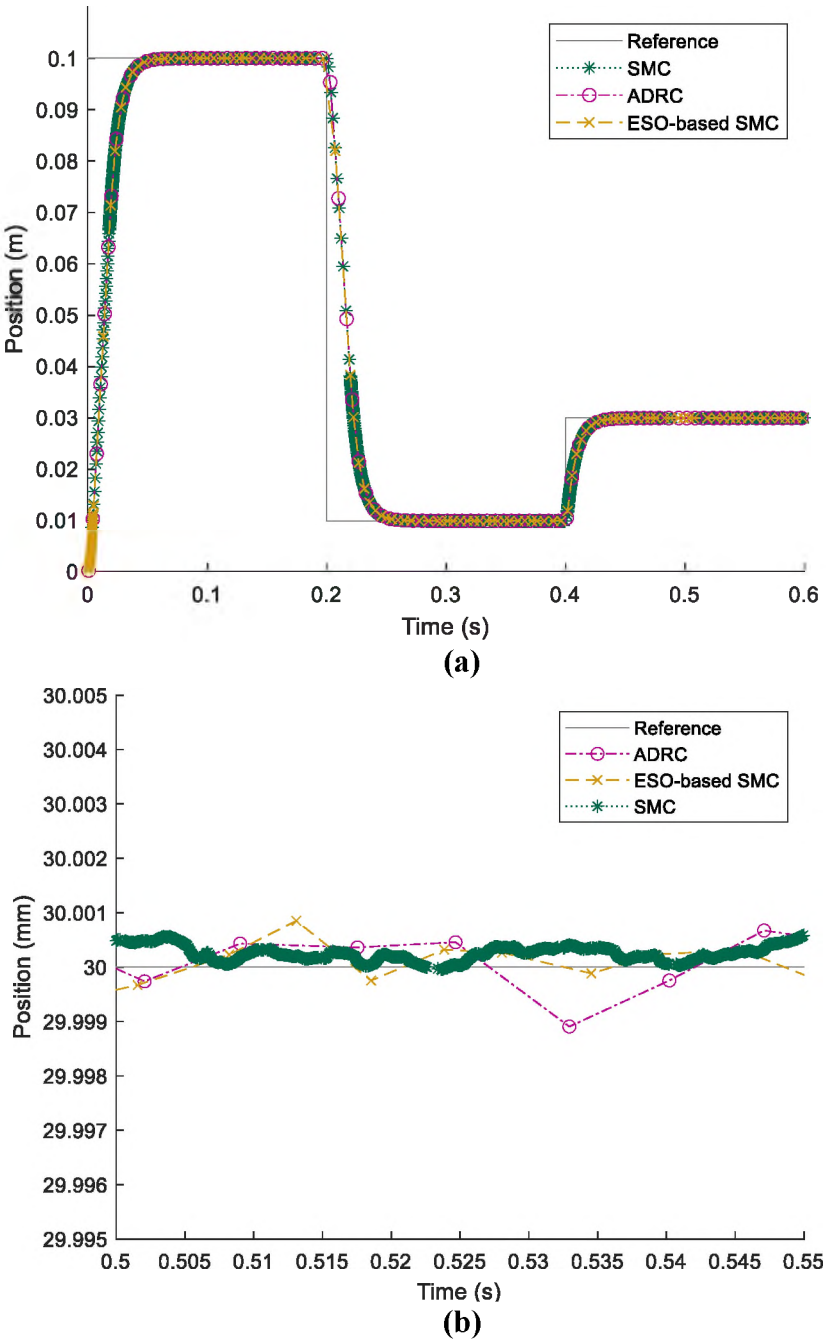

Figure 22: (a) Piston Position (b) Zoomed in Position

While position is not directly regulated by the controller, it is a direct outcome of the controlled pressures in each chamber. Pressure is related to position by (1) through the

force difference in each chamber. Figure 22 (a)-(b) indicate that there is good position tracking ability of all the controllers. Each controller correctly regulates the output position to the reference positions.

The steady state error (SSE) of position for each controller is shown in Figure 23. This is the position error for the timeframe of 0.45 seconds to 0.6 seconds when the position is commanded to 0.03 m. From Figure 24 we can see the SSE of each controller, however, the figure can be misleading. The average SSE for ADRC is 4.2×10^{-9} m, for ESO-based SMC is 2.5×10^{-8} m, and for SMC is -1.7×10^{-7} m. While SMC looks like the best SSE, it is consistently below the desired value, which causes the highest average error. ESO-based SMC fluctuates, but provides the least amount of average error.

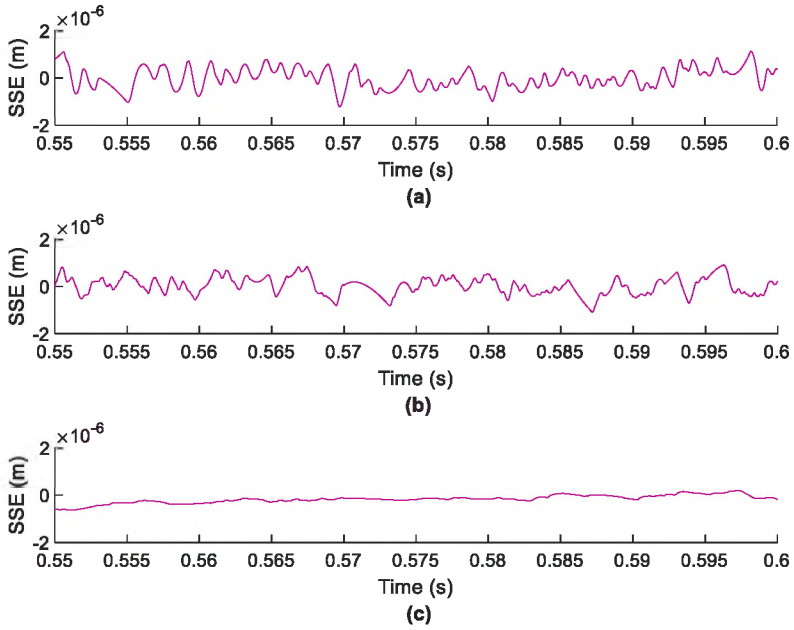

Figure 23: Steady State Error of (a) ADRC (b) ESO-based SMC and (c) SMC Controllers

2) Force Regulation: Force control is another key goal of this system design with impedance control. Since the goal of impedance control is to regulate force and

position, when the system has no environmental forces, the controller acts as if it is just a position controller. The interaction force, F_D, at the end of rod is depicted in Figure 24 for motion in free space. At steady state, the force is always zero. The force shown in this graph is derived from the pressure difference in the two chambers, so when the system is moving there is a non-zero force because the pressures are changing. It can be concluded from Figure 24 that all three controllers correctly and similarly regulate the force of the piston. All three controllers regulate the net force to zero in steady state.

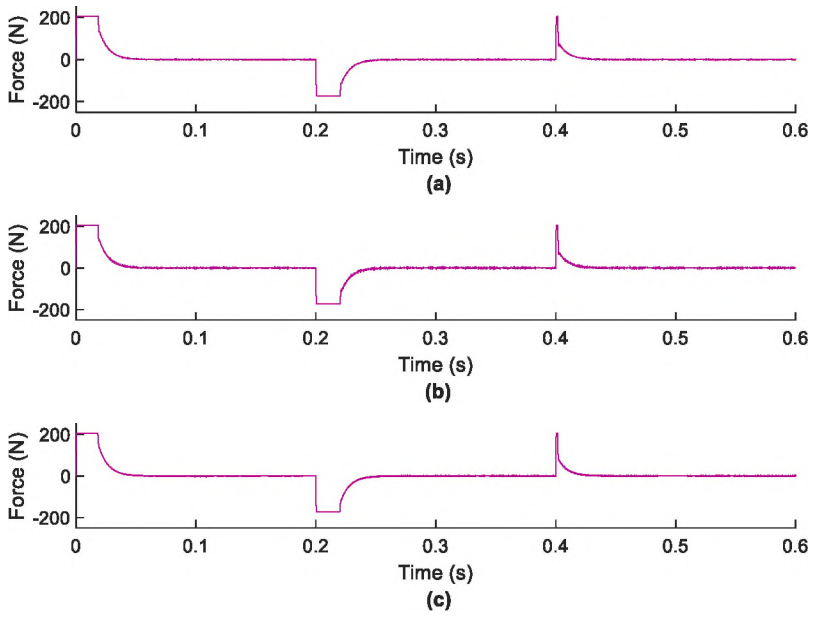

Figure 24: Controller Force of (a) ADRC (b) ESO-based SMC and (c) SMC

3) Chamber Pressure: Chamber pressures, P_1 and P_2 from (21), are what drive the position and force of the actuator. The pressure in an individual chamber relates directly to the force that the chamber puts on the separating disc between the two chambers. A non-zero force will move the actuator in a direction, while a net zero force will keep the actuator at its current location. Figure 25 is the three pressure charts, each detailing the simulated

pressure of each chamber as compared to the desired pressure output of the Impedance Control module.

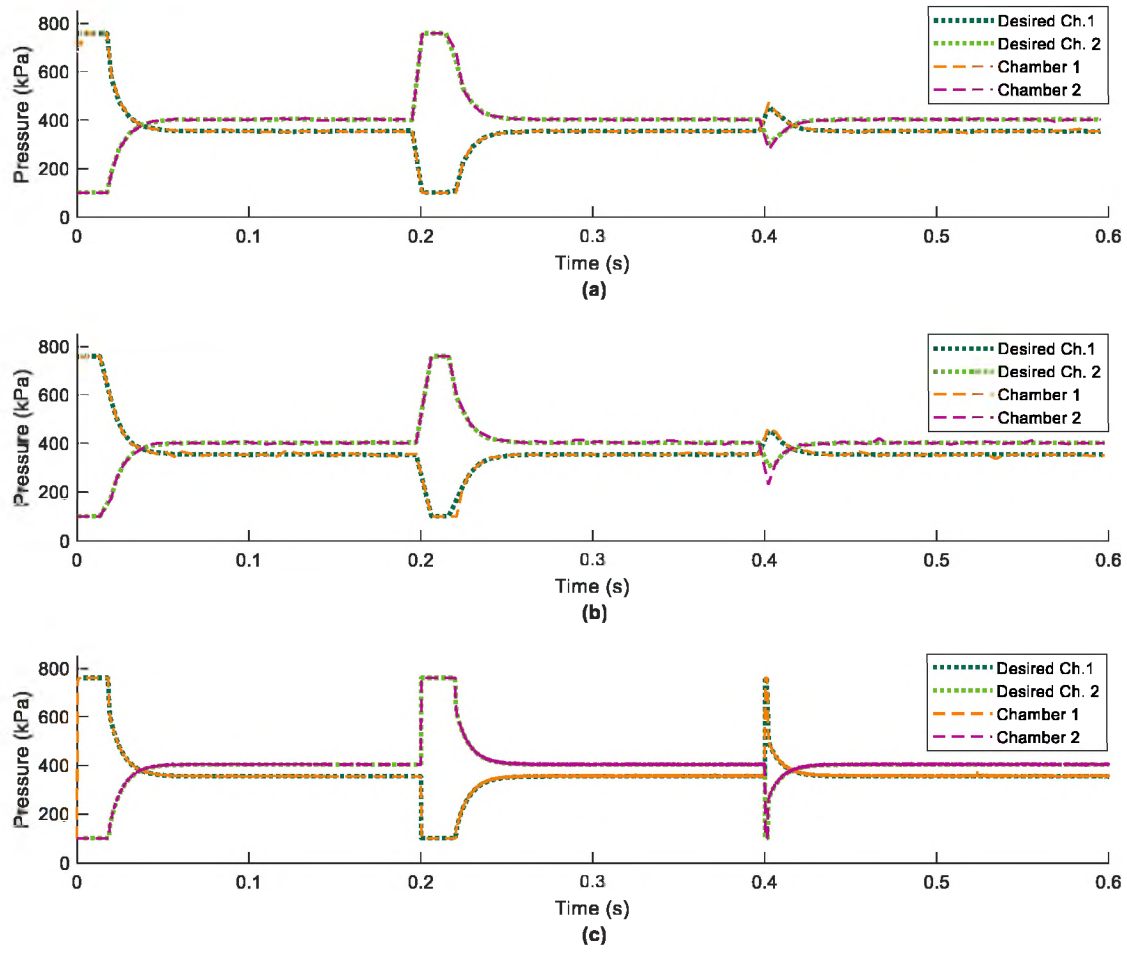

Figure 25: Desired and Actual Chamber Pressure for (a) ADRC (b) ESO-based SMC and (c) SMC

As expected, the pressure stays constant when position is constant and the pressure changes accordingly as position changes. The pressure into each chamber is determined by the mass flow rate of the pair of discrete control valves that regulates the flow of air into and out of the respective chamber. From Figure 25 we can see that the pressure output under the control of SMC shows the smoothest response compared to the other two.

4) Valve Excitation: The discrete control valves manage the pressure in a respective chamber. The valves use the output of the control system, a mass flow rate, to determine if pressure should be added or removed from the chamber. The use of discrete valves was a goal of this research; however, the triggering of the valves must be observed. The control signals that are utilized to excite the valves in chamber 1 are shown in Figure 26. The excitations of these valves must be scrutinized since they will wear and degrade the mechanical parts over time. It is noticed from Figure 26 that ADRC and ESO-based SMC outperform SMC in valve control. Valves 1 and 2 for ADRC excite 833 times, for ESO-based SMC the valves excite 910 times, and for SMC the valves excite 40,905 times. ADRC does perform slightly better than the other controllers in this instance.

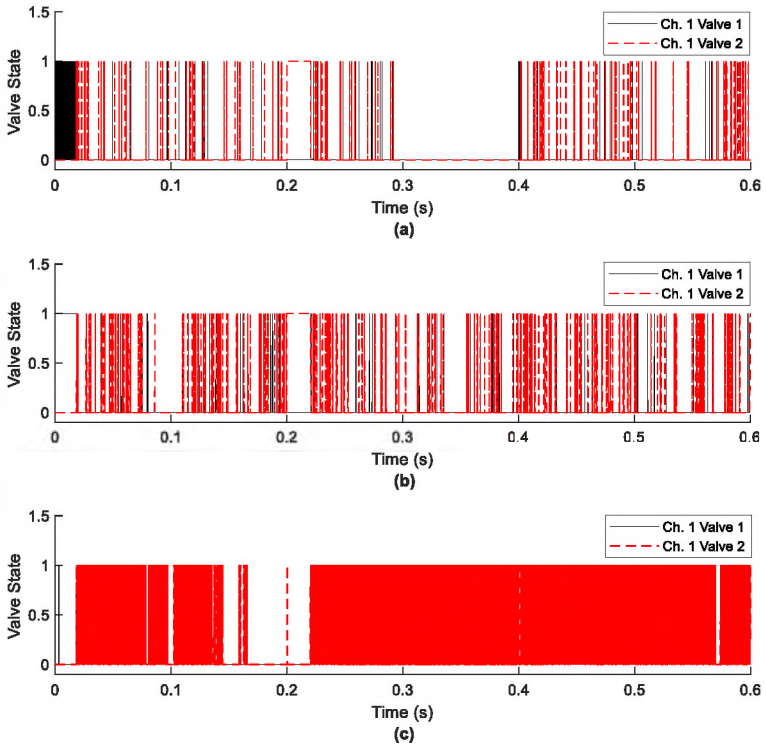

Figure 26: Valve States in Chamber 1 under the Control of (a) ADRC (b) ESO-based SMC and (c) SMC

5) *Control Effort*: The control effort, which determines the valve response for each chamber, is demonstrated in Figure 27. This is a representation of how hard the specific controller must work in order to regulate the output pressure of each chamber to the desired level and allow it to remain at the desired level. ADRC used the least amount of control effort to accomplish the control goals, with ESO-based SMC needing slightly more effort, and SMC using the most control effort.

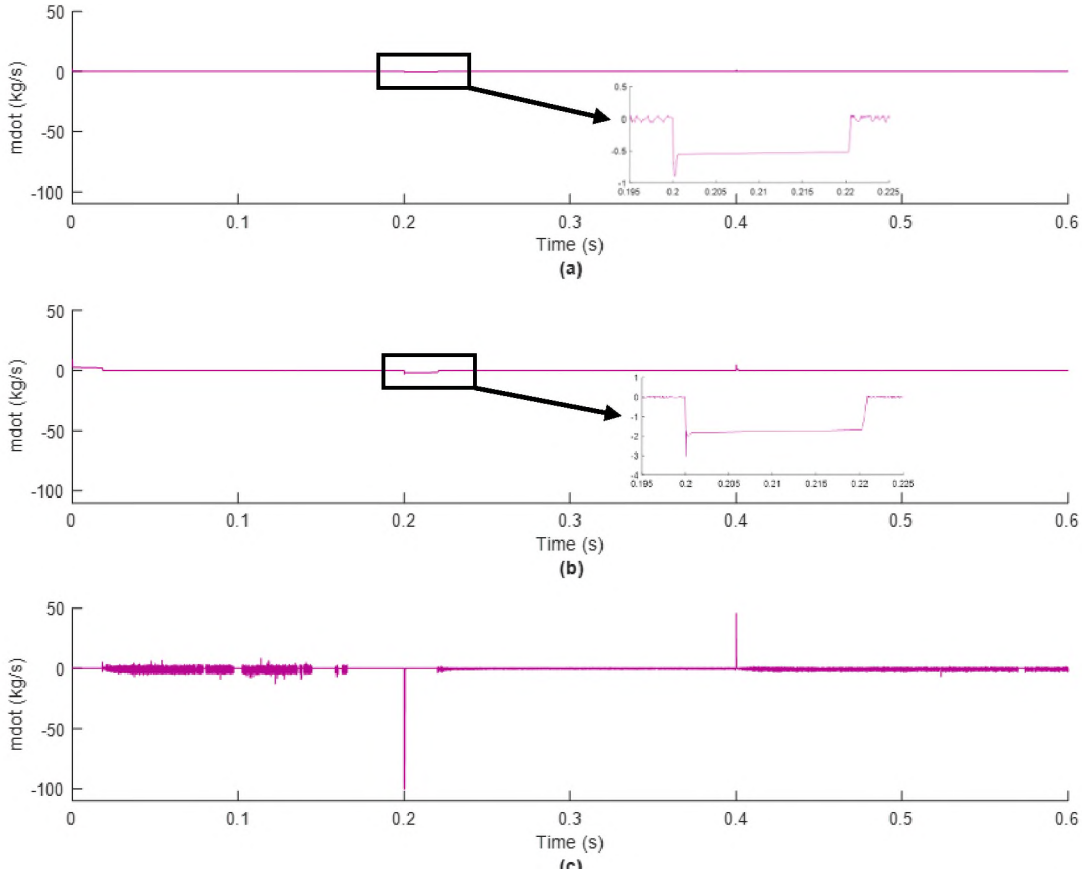

Figure 27: Control Effort of (a) ADRC (b) ESO-based SMC and (c) SMC

6) *Pressure Estimation by ESO*: Lastly, the estimation of the extended state observer for the two controllers that use it, ADRC and ESO-based SMC, is displayed in Figure 28. This plot shows the observer's ability to estimate the pressure in the system,

allowing the controller's performance not to be affected by this variation in the system. The pressure estimation in ADRC better estimates the pressure than ESO-based SMC. ADRC provides a smoother pressure result than that of ESO-based SMC.

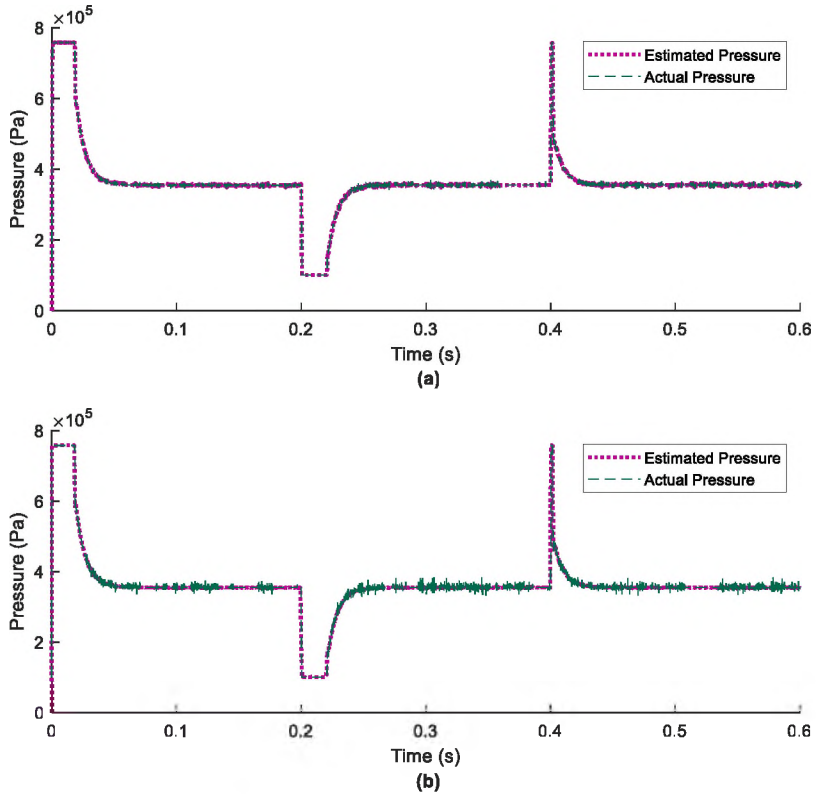

Figure 28: Pressure Estimation Comparison between (a) ADRC and (b) ESO-based SMC

7) Noncontact to Contact Transition: Impedance control is mainly used to regulate the relationship between force and position of the piston when the piston encounters something in the environment unexpectedly that inhibits its motion in some way. This is based on the imposed force and the impedance control design. In this thesis, the system is commanded to a position of 0.1 m. However, at 0.08 m there is a stiff object

that prevents the piston from moving further. In this research, it was thought of as a wall, but it could be any similar object. As is seen in Figure 29, the piston position is stopped at 0.08 m between 0 and 0.2 seconds even though the desired position was 0.1 m. There is thus a non-zero force applied by the actuator that is equal to the force applied by the object as seen in Figure 30. The force limitation of the actuator comes from both the maximum pressure supplied and any physical limitations of the hardware. Figure 29 shows the actuator's response to this unknown object. All three controllers show comparable responses in accomplishing this goal.

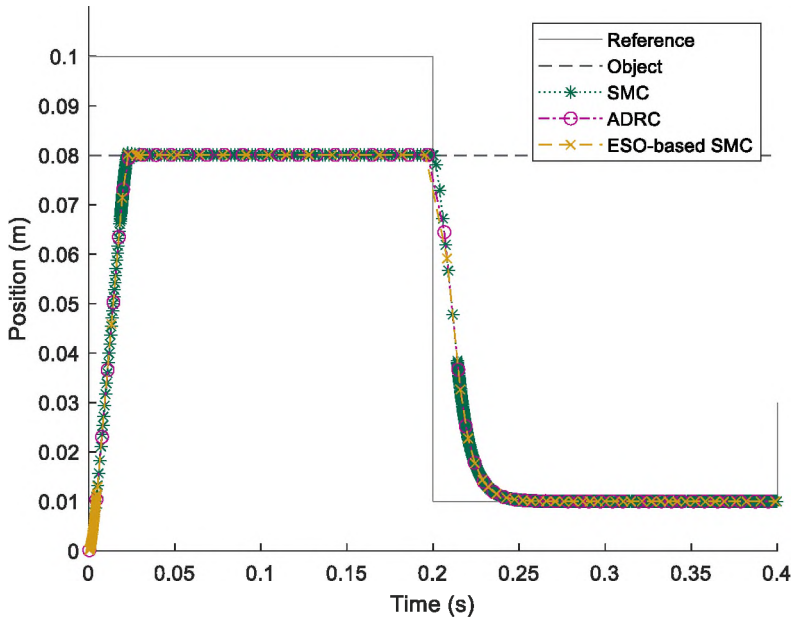

Figure 29: Piston Position with Unexpected Object at 0.08 m

As can be seen in Figure 30, the piston exerts a non-zero force at the point where the piston encounters the object. In comparison to Figure 24, the force in steady state is normally zero. This is true when the piston is commanded back to 0.01 m. Thus, all three controllers are comparable in correctly accomplishing the task of exerting a net-zero force by producing a force proportional to the environmental force from 0-0.2 seconds. There is

a slight dip in the force at approximately 0.025 seconds. This is the point at which the actuator encounters the wall and is compensating for the disturbance accordingly and then regulates back to the desired force.

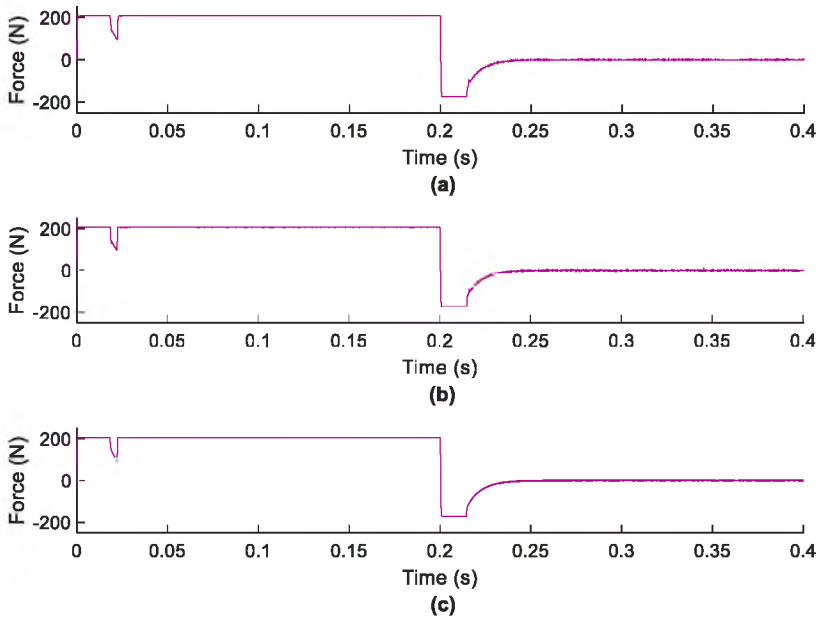

Figure 30: Piston Force with Unexpected Object from (a) ADRC (b) ESO-based SMC and (c) SMC

The pressure result for the transition to a contact force is shown in Figure 31. It is seen that the chamber pressure for chamber 1 is equal to P_{sum} and the pressure for chamber 2 is equal to P_{atm} during the contact time of approximately 0.03 to 0.2 seconds. All controllers produce similar and acceptable results to produce this non-zero result when external force is encountered. This is expected and desired since the environmental force is causing the piston to exert all its possible force. This is accomplished by fully pressurizing chamber 1 and fully evacuating chamber 2 so that it is at atmospheric pressure.

Lastly, the valve state for each controller is shown in Figure 32. This shows how the valves for chamber 1 react to the additional force requirement and the unexpected position change. ESO-based SMC succeeds slightly better than ADRC in producing the least valve excitation in order to regulate the chamber pressure, actuator force, and piston position. In this simulation, the ESO-based SMC valves for chamber 1 excited 493 times, the ADRC valves excited 981 times, and the SMC valves excited 21,593 times.

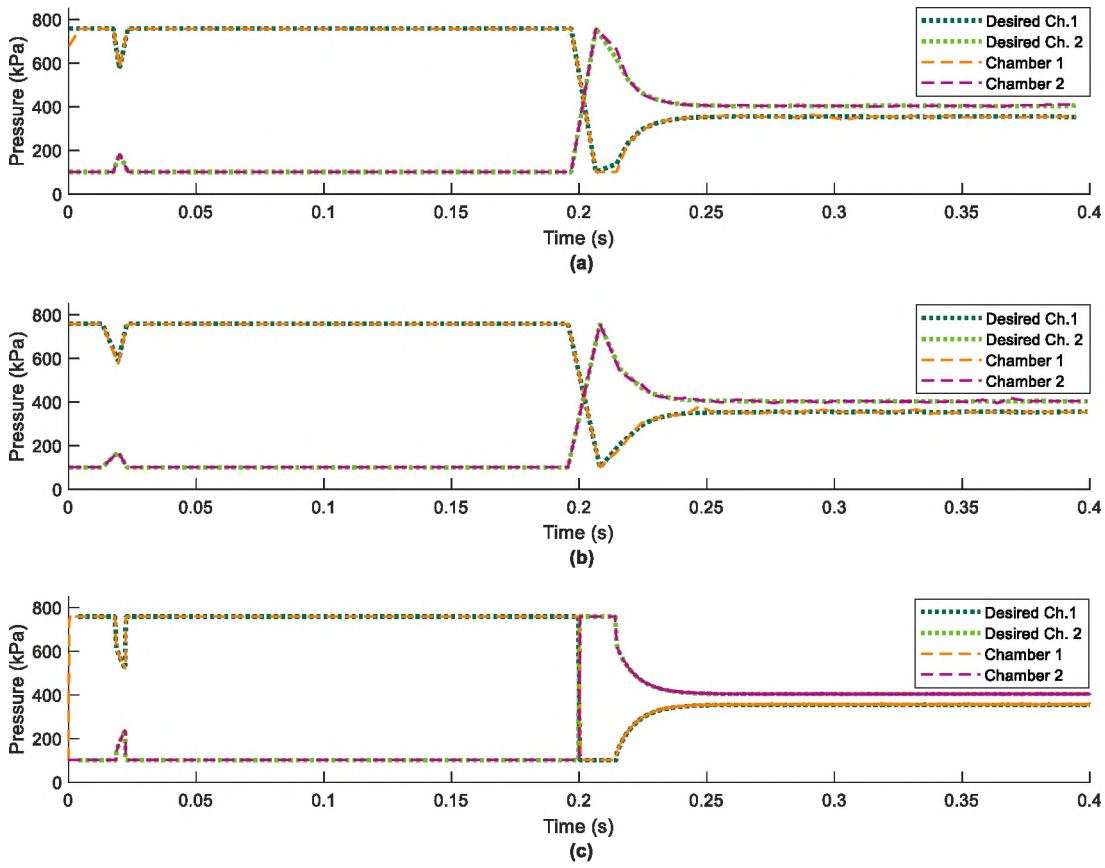

Figure 31: Chamber Pressure with Unexpected Object under the Control of (a) ADRC (b) ESO-based SMC and (c) SMC

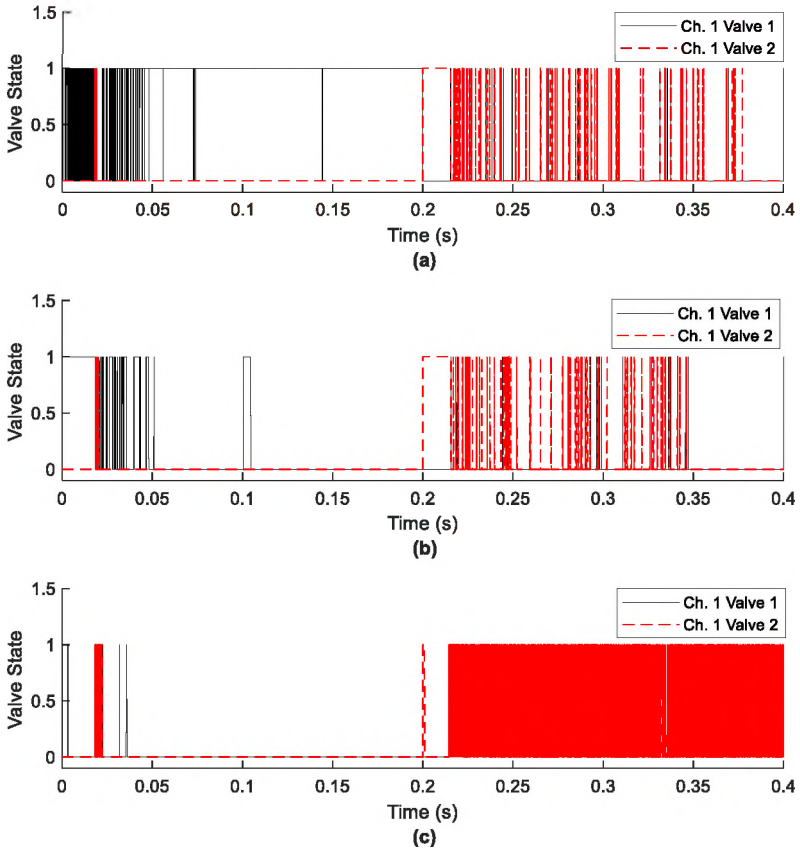

Figure 32: Chamber 1 Valve States with Environmental Force for (a) ADRC (b) ESO-based SMC and (c) SMC

8) Parameter Variations: The impedance parameters are varied, as shown in Figure 33, with $\widetilde{K}$ increased by 1%, $\widetilde{M}$ reduced by 80%, and $\widetilde{B}$ varied 124% so that the system remains critically damped. The result is still a system that commands the piston to the desired positions. However, there is a slight difference between Figure 33(a) and Figure 22(a) as the settling times are different between the impedance models. This is expected, however, due to the difference in time constant of the Mass-Spring-Damper system in the impedance control module. All three controllers still correctly regulate the piston position, but with a slightly slower settling time, as expected. Both are critically damped systems, but this latter system has a slightly higher time constant and consequently takes a little

more time to reach the desired position. This new model response has a settling time of 0.0409 seconds, which is more than double the original settling time.

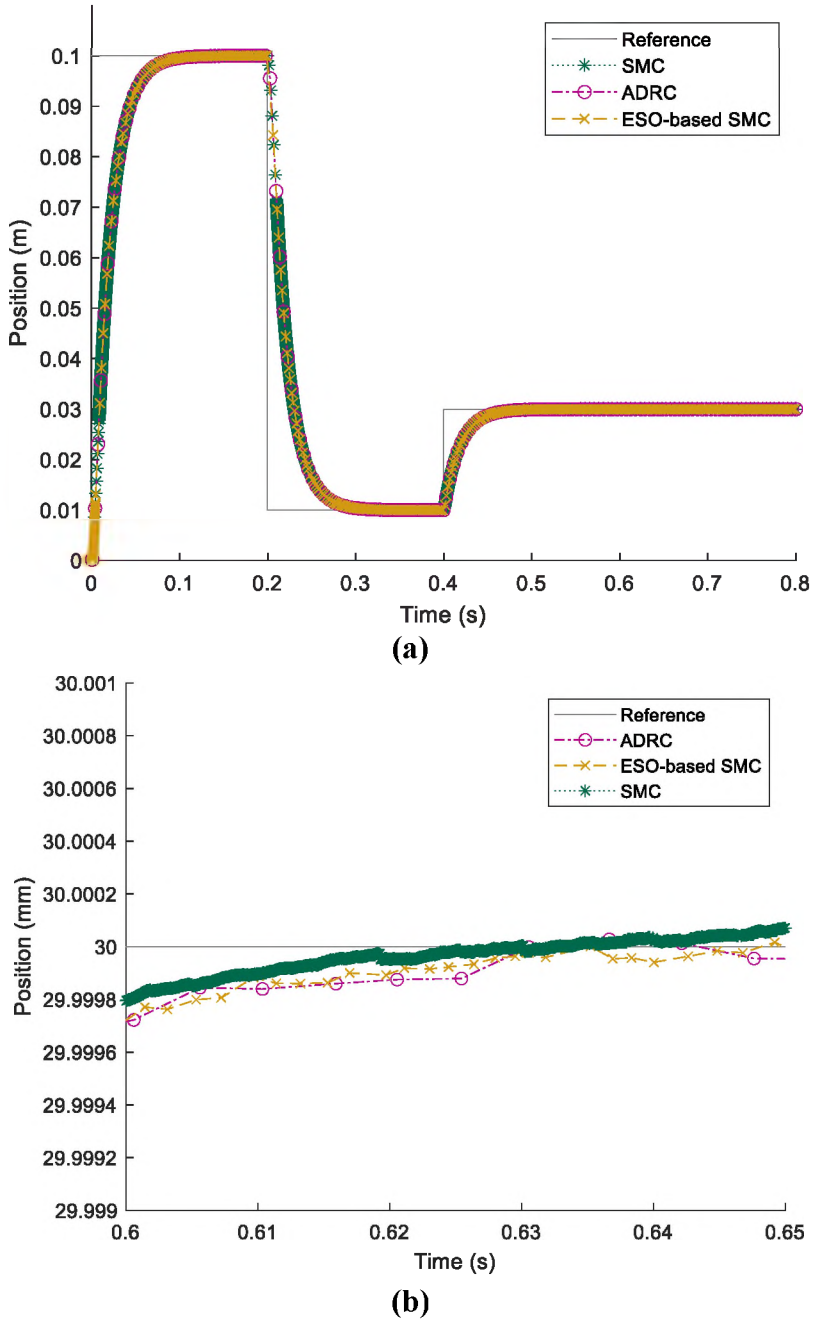

Figure 33: Positions Outputs with Parameter Variations (a) Position Outputs and (b) Transient Response

The resulting chamber pressure and control effort for the new parameters are shown in Figure 34 and Figure 35, respectively, for further comparison with the companion graphs above for the original parameters. SMC in Figure 34 produces a pressure output that is not as smooth as the original, and ADRC and ESO-based SMC provide comparable outputs. ADRC uses the least control effort in Figure 35. Both of these results are like the original results as shown in Figure 25. So, we can conclude that there is little effect of parameter variation on the response to the system.

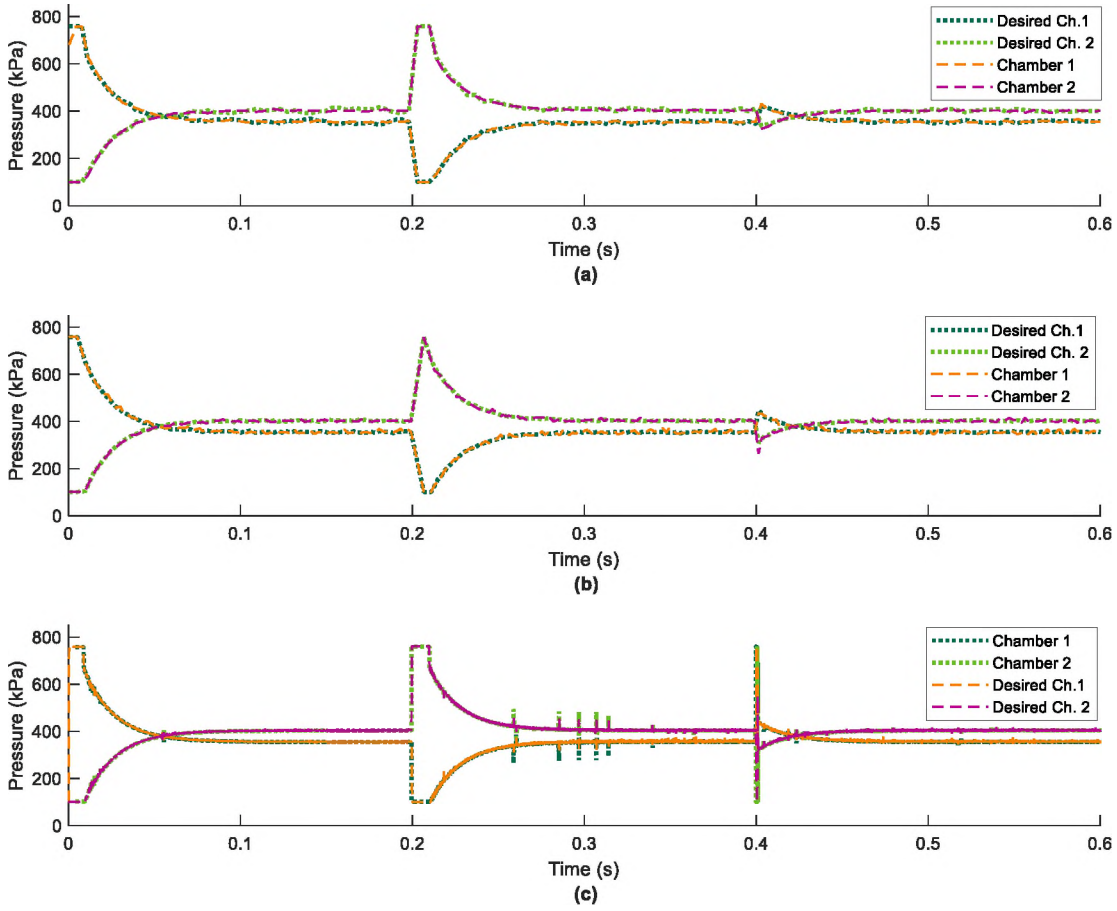

Figure 34: Chamber Pressure Based on New Parameters for (a) ADRC (b) ESO-based SMC and (c) SMC

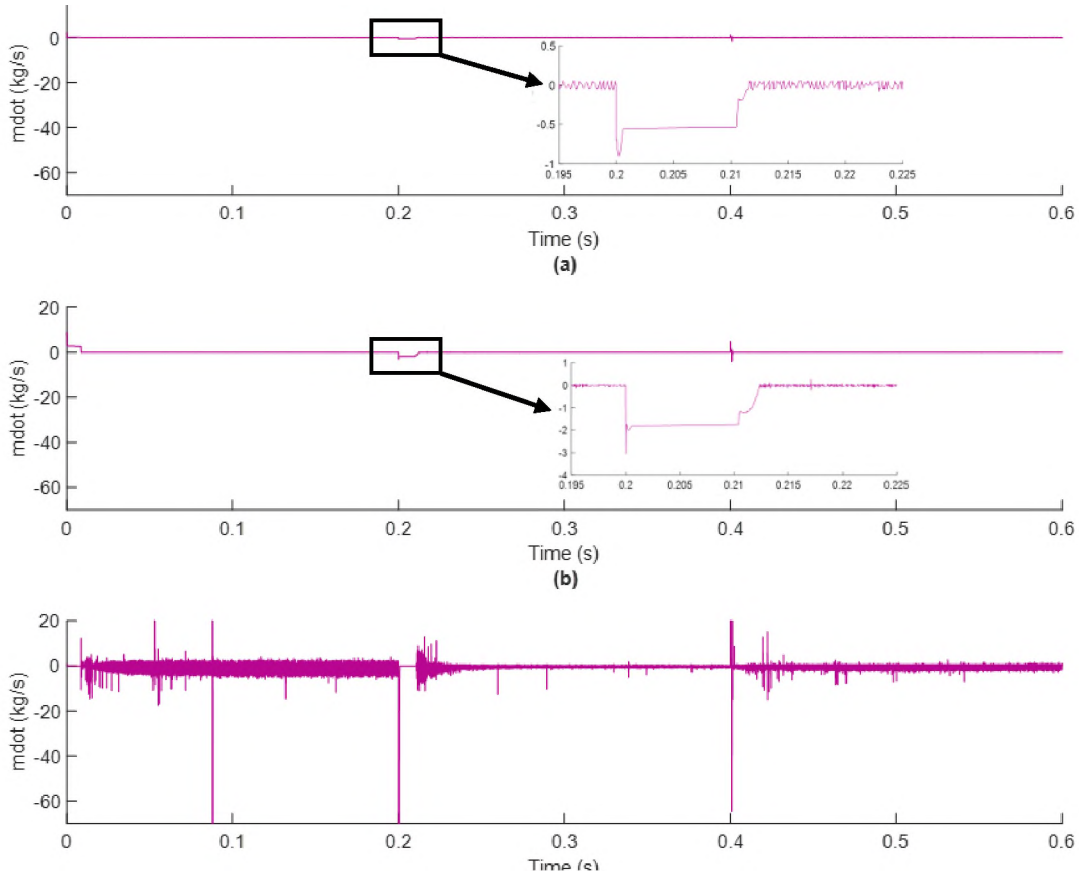

Figure 35: Control Effort based on New Parameters for (a) ADRC (b) ESO-based SMC and (c) SMC

The force regulation for the parameter varied response is shown in Figure 36 and produced similar results to the force regulation in the original simulation shown in Figure 24. The force in Figure 36 is F_L. In comparing to the original force regulation in Figure 24, the results of all three controllers are still comparable.

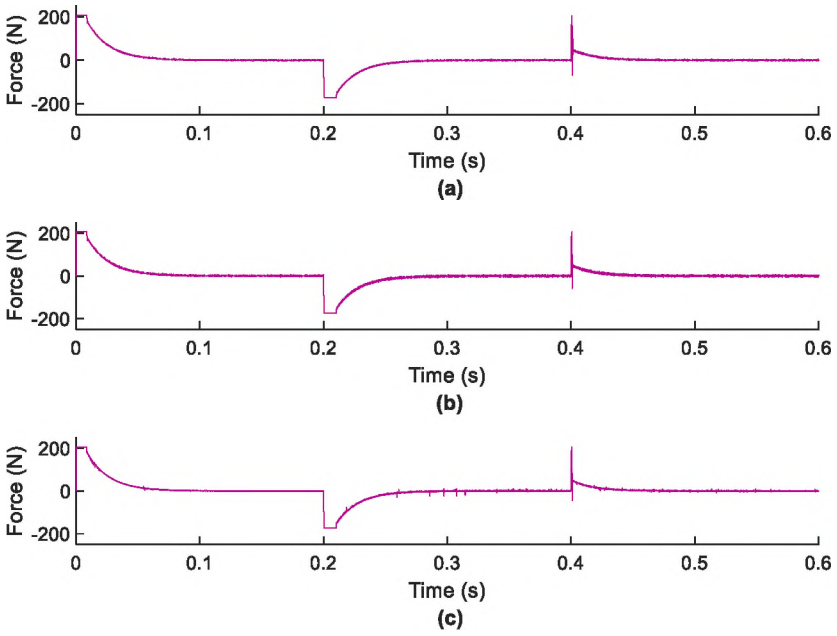

Figure 36: Force Regulation for Parameter Variation in (a) ADRC (b) ESO-based SMC and (c) SMC

9) Controller Robustness Comparison: Figure 37 shows the effect of a constant input disturbance on position. The disturbance is a step disturbance of -2 kg/s and added to the input of the pressure module at 0.5 seconds for chamber 1. The disturbance represents a sudden leak within the system. It could be a loose connection, a hole in the tubing, or wear to a seal on the pneumatic actuator. The purpose of this is to show the robustness of the controller when there is input disturbance. A reference signal shows the commanded position versus the actual position of the three controllers. Observing Figure 37(b), we find that the ADRC and ESO-based SMC controllers are robust enough to compensate for this sudden change without any detriment to position. However, the SMC controller shows a steady-state error in position of approximately 0.01 mm after the disturbance is added to the system. The chamber pressure and control effort are detailed in

Figure 38 and Figure 39, respectively, to elucidate how the system responds to this disturbance.

Figure 38 does not show any noticeable change when compared to Figure 25. This means that all three controllers are robust enough to compensate for the change of mass flow rate in the system. However, the side-effect of this is noticed in Figure 40. To compensate for this leak in chamber 1 at 0.5 seconds, valve 1, which supplies system pressure to chamber 1, needs to excite rapidly in order to keep the pressure at the desired value.

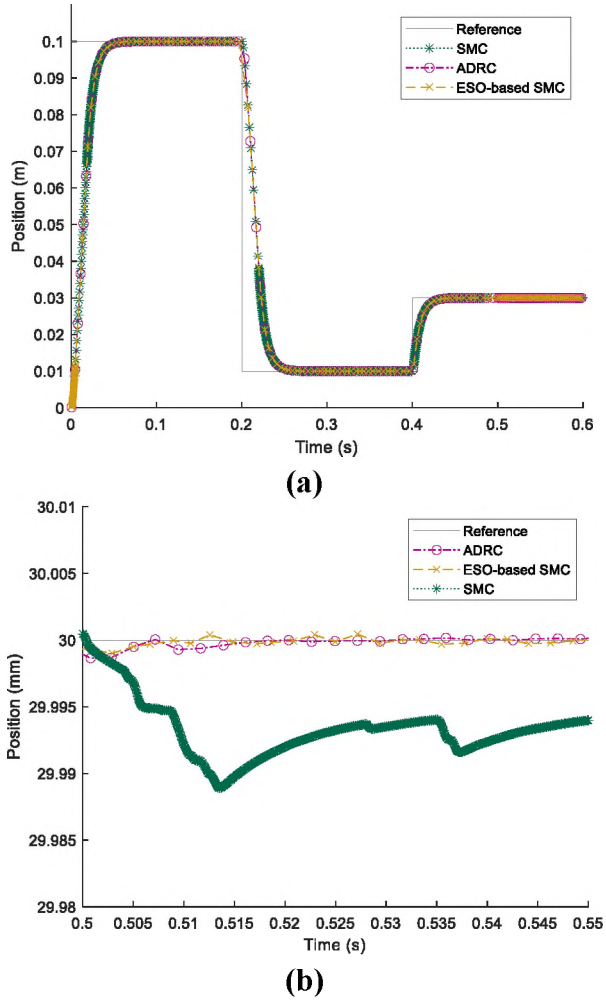

Figure 37: Position Outputs with Input Disturbance (a) Position Result (b) Zoom-in View as t= 0.5 seconds

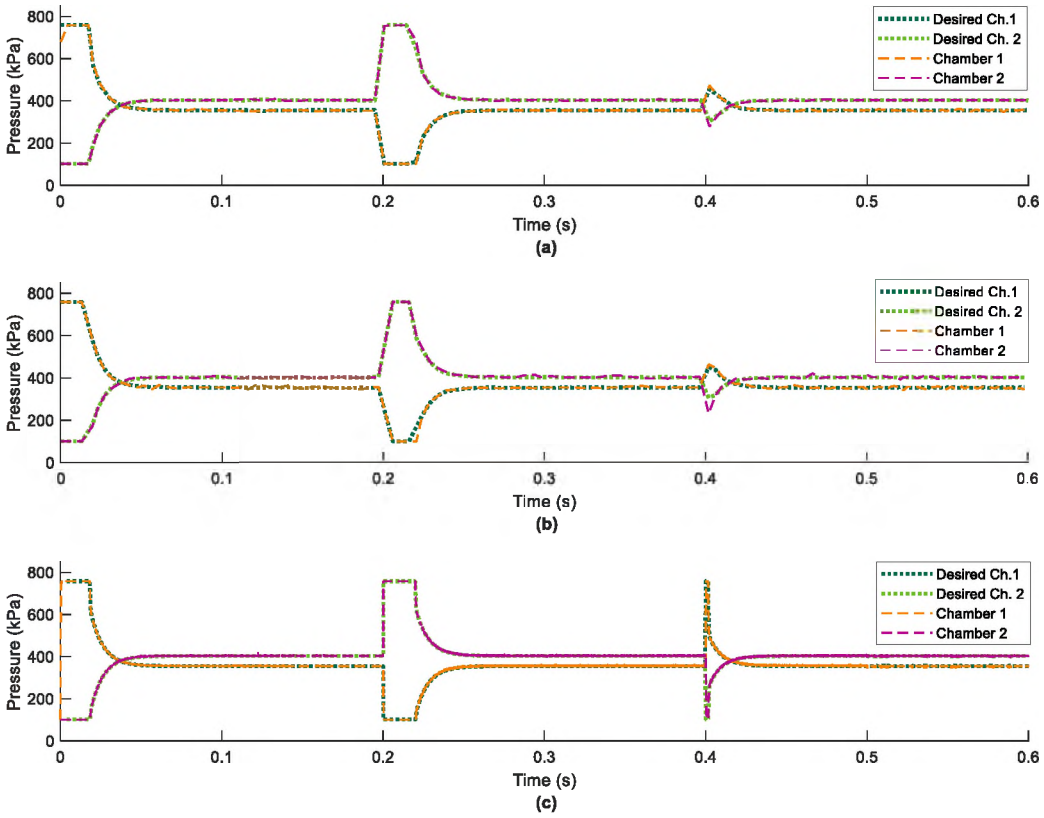

Figure 38: Chamber Pressures with Disturbance Input of (a) ADRC (b) ESO-based SMC and (c) SMC

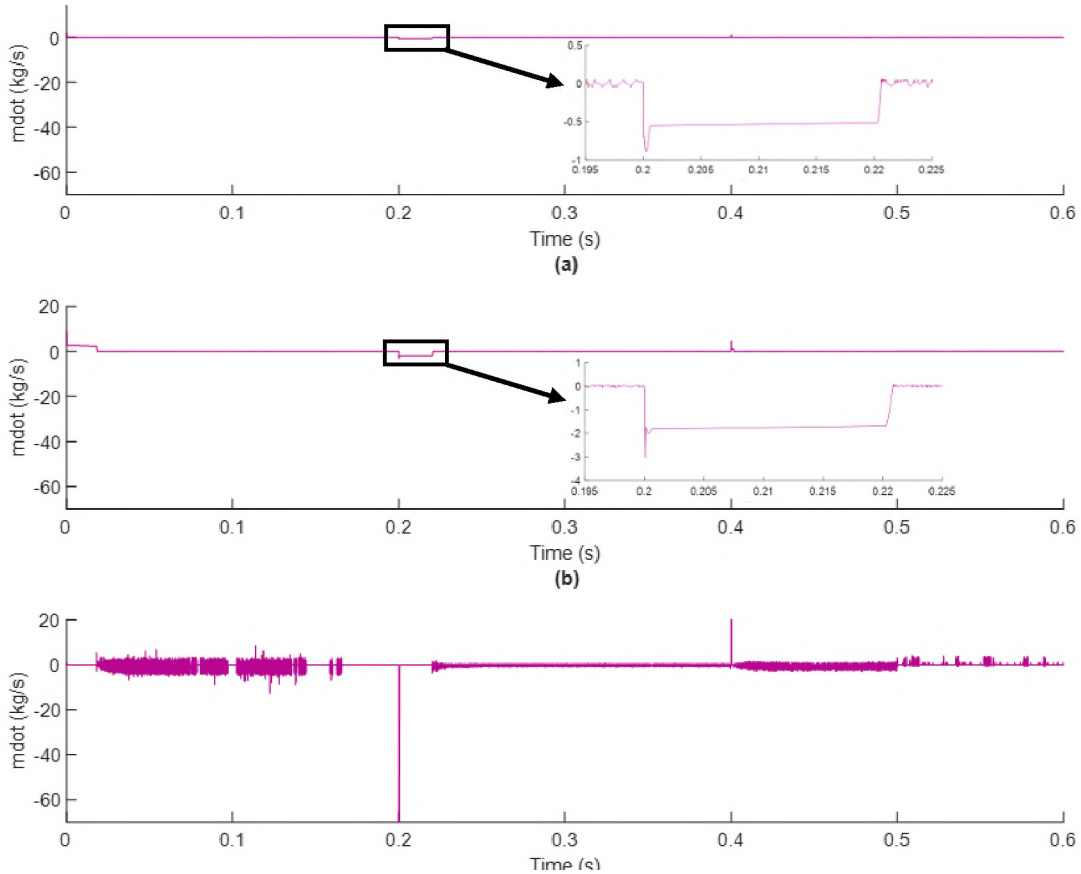

Figure 39: Control Effort with disturbance input for (a) ADRC (b) ESO-based SMC and (c)SMC

The control effort for chamber 1, detailed in Figure 39, stays similar to the normal control effort detailed in Figure 27. ADRC produces the least amount of effort in order to complete the task. However, each controller used more control effort once the leak was introduced. This is seen in Figure 40 where at 0.5 seconds the valve states become very dense as the controller tries to regulate and keep the pressure at the desired value. For this simulation, the chamber 1 valves for ADRC excited 2,379 times, the chamber 1 valves for ESO-based SMC excited 2,712 times, and the chamber 1 valves for SMC excited 48,169 times.

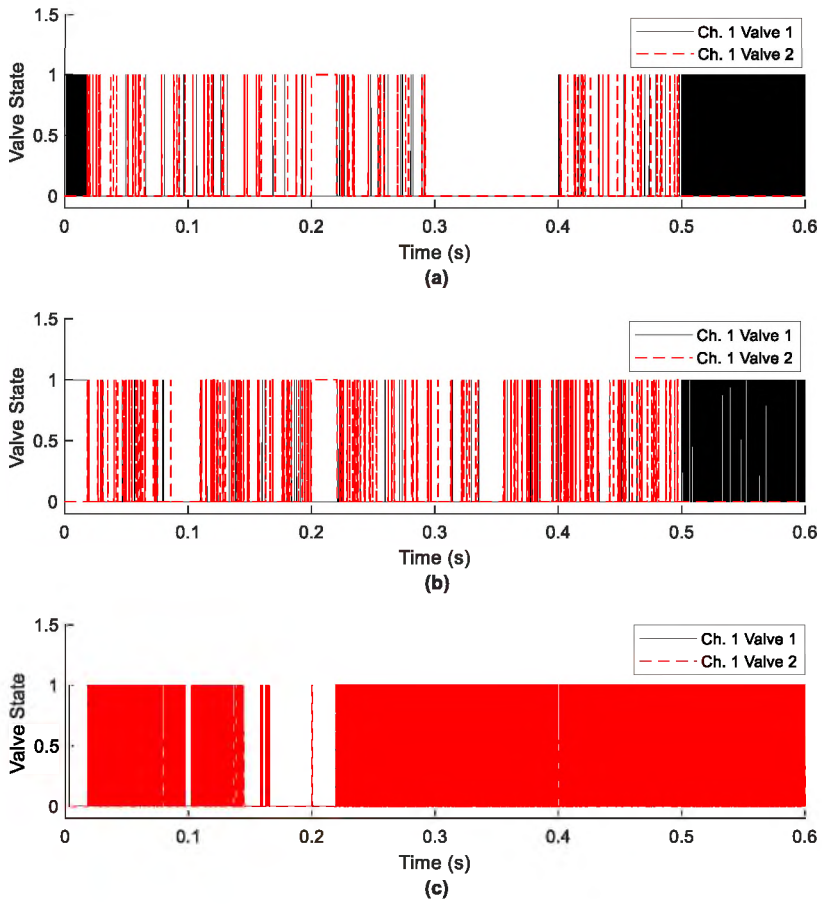

Figure 40: Chamber 1 Valve States with Disturbance Input for (a) ADRC (b) ESO-based SMC and (c) SMC

C. Discussion

In summary, ADRC produced the best overall results by first meeting all the control goals of the system in non-contact and contact motion. It also performed well when parameters were varied and in the presence of a disturbance. It consistently produced the least overall control effort and least valve excitation to accomplish these goals.

CHAPTER V

CONCLUSION

A. Conclusion

The goal of this thesis was to use impedance control for a linear pneumatic actuator in order to regulate the relationship between the force and position of the system. To accomplish this, advanced nonlinear control techniques were necessary to regulate the pressure in each chamber of the actuator. Three different methods of control were simulated, ADRC, ESO-based SMC, and SMC, in order to compare the results. While SMC has been predominately used in impedance control, neither ADRC nor ESO-based SMC have been extensively used in pressure tracking. When SMC is used for pressure tracking, non-conventional sliding surfaces are typically used since they provide better tracking, such as in [13], or a force equation is used to control the system such as in [16]. However, for this thesis, a first order SMC was developed to demonstrate how the ADRC and ESO-based SMC models improved on this first method.

SMC accomplished all the control goals desired, but did so with large control effort, relatively speaking, and with many valve excitations. Thus, the SMC design in this thesis was not conducive to practical application. So, the next step taken was to design an ESO-based SMC controller for this application. The addition the ESO eliminated the need for

the controller to use the actual position and velocity feedback from the plant by instead estimating disturbance and model uncertainty. The ESO state vector was then incorporated into the SMC control law. Also, this controller used an estimate for the control gain instead of an actual calculation, due again to the removal of the position and velocity feedback. ESO-based SMC did improve the control effort and valve excitation while still meeting all of the control goals. Lastly, ADRC was designed to accomplish the same control goal. This system used the ESO and estimate of the control gain from ESO-based SMC. However, instead of a plant-based model, this control law was based solely on a proportional controller that does require the accurate model of the system. It is demonstrated in simulation results that ADRC produced the best results. This is due to the robust disturbance rejection in the ESO that treats all unknown parts of the plant as a disturbance and estimates it. In addition, the use of a proportional controller compensates the disturbance in real time, producing desired results.

B. Future Work

The proposed research is based on the force in a pushing motion. In the future, we can investigate the control problems associated with both push and pull motions, as if the piston has grasped an object or is physically linked to the object and it is moving it.

This thesis also focused on the impedance control aspect of a pneumatic actuator system with discrete valves. A next step in this process would be to better model and control these discrete valves so that switching can be even further reduced for industrial applications.

Impedance control could also be studied more to understand if the position and velocity feedback from the system is needed, or if it could possibly be estimated. While

position and velocity feedback has been eliminated in the pressure controller portion, it is still needed for the impedance control portion. However, velocity is not always easy to measure in practice. So, if this were eliminated from the system, it could provide further reduction in physical components needed.

Lastly, the next logical step for this work is to implement these controllers with hardware. These same simulations will be performed again with physical hardware to compare the efficacy and performance of these systems. It will also show if the models provide realistic simulations of the actual system.

REFERENCES

[1] "A Brief History Of Linear Actuators," Progressive Automations, 30 May 2018. [Online]. Available: https://www.progressiveautomations.com/blogs/news/brief-history-linear-actuators. [Accessed 21 10 2019].

[2] C. Gonzalez, "What's the Difference between Pneumatic, Hydraulic, and Electric Actuators?," Machine Design, 16 April 2015. [Online]. Available: https://www.machinedesign.com/linear-motion/what-s-difference-between-pneumatic-hydraulic-and-electrical-actuators. [Accessed 21 10 2019].

[3] "Know Your Pneumatics: Single or Double Acting? Choosing the Right Cylinder," Parker, 26 9 2017. [Online]. Available: http://blog.parker.com/know-your-pneumatics-single-or-double-acting-choosing-the-right-cylinder. [Accessed 21 10 2019].

[4] T. Driver and X. Shen, "Pressure Estimation-Based Robust Force Control of Pneumatic Actuators," *International Journal of Fluid Power,* vol. 14, no. 1, pp. 37-45, 2013.

[5] P. Zhang, "Transducers and valves," in *Advanced Industrial Control Technology*, 2010, pp. 117-152.

[6] E. Richer and Y. Hurmuzlu, "A High Performance Pneumatic Force Actuator System: Part I—Nonlinear Mathematical Model," *ASME. J. Dyn. Sys., Meas., Control,* vol. 122, no. 3, pp. 416-425, 2000.

[7] H. Kazerooni, "Design and Analysis of Pneumatic Force Generators," *IEEE/ASME Transactions on Mechatronics,* vol. 10, no. 4, pp. 411-418, 2005.

[8] P. G. Harris, G. E. O'Donnell and T. Whelan, "Modelling and identification of industrial pneumatic drive system," *The International Journal of Advanced Manufacturing Technology,* vol. 58, no. 9-12, pp. 1075-1086, 2011.

[9] J. Swevers, F. Al-Bender, C. Ganseman and T. Projogo, "An integrated friction model structure with improved presliding behavior for accurate friction compensation," *IEEE Transactions on Automatic Control,* vol. 45, no. 4, pp. 675-686, 2000.

[10] A.-B. F. S. J. V. P. V. B. H. Nouri BMY, "Modelling a pneumatic servo positioning system with friction," in *Proceedings of the American control conference*, Chicago, 2000.

[11] M. Turkseven and J. Ueda, "Model-Based Force Control of Pneumatic Actuators With Long Transmission Lines," *IEEE/ASME Transactions on Mechatronics,* vol. 23, no. 3, pp. 1292-1302, 2018.

[12] W. Bolton, "Correction Elements," in *Instrumentation and Control Systems*, 2015, pp. 123-150.

[13] Y. Zhu and E. J. Barth, "Impedance Control of a Pneumatic Actuator for Contact Tasks," in *Proceedings of the 2005 IEEE International Conference on Robotics and Automation*, Barcelona, 2005.

[14] B. Taheri, D. Case and E. Richer, "Force and Stiffness Backstepping-Sliding Mode Controller for Pneumatic Cylinders," *IEEE/ASME Transactions on Mechatronics,* vol. 19, no. 6, pp. 1799-1809, 2014.

[15] C. Ying, J.-f. Zhang, Y. Can-jun and N. Bin, "Design and hybrid control of the pneumatic force-feedback systems," *Mecatronics,* vol. 17, no. 6, pp. 325-335, 2007.

[16] F. Najafi and B. Hejrati, "Impedance Control of a Pneumatic Actuator Using Fast Switching On/Off Solenoid Valves for Tasks Containing Contact," in *17th Annual International Conference on Mechanical Engineering*, Tehran, 2009.

[17] D. Saravanakumar, B. Mohan and T. Muthuramalingam, "A review on recent research trends in servo pneumatic positioning systems," *Precision Engineering,* vol. 49, pp. 481-492, 2017.

[18] K. e. a. Song, "Pneumatic actuator and fexible piezoelectric sensor for soft virtual reality glove system," *Scientific Reports,* vol. 9, no. 1, pp. 1-8, 2019.

[19] A. Koivikko, E. S. Raei, M. Mosallaei, M. Mäntysalo and V. Sariola, "Screen-Printed Curvature Sensors for Soft Robots," *IEEE Sensors Journal,* vol. 18, no. 1, pp. 223-230, 2018.

[20] X. Luo, J. Wang, H. Sun, J. W. Derby and S. J. Mangan, "Study of a New Strategy for Pneumatic Actuator System Energy Efficiency Improvement via the Scroll Expander Technology," *IEEE/ASME Transations on Mechatronics,* vol. 18, no. 5, pp. 1508-1518, 2013.

[21] R. Richardson, A. R. Plummer and M. D. Brown, "Self-tuning Control of a Low-Friction Pneumatic Actuator Under the Influence of Gravity," *IEEE Transactions on Control Systems Technology,* vol. 9, no. 2, pp. 330-334, 2001.

[22] Z. Rao and G. M. Bone, "Nonlinear Modeling and Control of Servo Pneumatic Actuators," *IEEE Transactions on Control System Technology,* vol. 16, no. 3, pp. 562-569, 2008.

[23] B. Rouzbeh, G. M. Bone and G. Ashby, "High-Accuracy Position Control of a Rotary Pneumatic Actuator," *IEEE/ASME Transactions on Mechatronics,* vol. 23, no. 6, pp. 2774-2781, 2018.

[24] X. Shen and M. Goldfarb, "Simultaneous Force and Stiffness Control of a Pneumatic Actuator," *Journal of Dynamic Systems, Measurement, and Control,* vol. 129, no. July 2007, pp. 425-434, 2007.

[25] S. Hodgson, M. Tavakoli, M. T. Pham and A. Leleve, "Nonlinear Discontinuous Dynamics Averaging and PWM-Based Sliding Control of Solenoid-Valve Pneumatic Actuators," *IEEE/ASME Transactions on Mecatronics,* vol. 20, no. 2, pp. 876-888, 2015.

[26] Q. M. Le, M. T. Pham, M. Tavakoli, R. Moreau, J.-P. Simon and T. Redarce, "Bilateral Control of Nonlinear Pneumatic Teleoperation System with Solenoid Valves," *IEEE Transactions on Control Systems Technology,* vol. 21, no. 4, pp. 1463-1470, 2013.

[27] N. Hogan, "Impedance Control: An Approach to Manipulation: Part II - Implimentation," *Transactions of ASME,* vol. 107, no. March, pp. 8-16, 1985.

[28] A. Goswami and P. Vadakkepat, "Compliance/Impedance Control Strategy for Humanoids," in *Humanoid Robotics: A Reference*, Springer, Dordrecht, 2017.

[29] T. Kurfess, Impedance and Interaction Control, CRC Press, 2005, pp. 19-1 - .

[30] S. Kumar, V. Rastogi and P. Gupta, "A hybrid impedance control scheme for underwater welding robots with a passive foundation in the controller domain," *Simulation: Transactions of the Society for Modeling and Simulation International,* vol. 93, no. 7, pp. 619-630, 2017.

[31] N. Garmsiri, Y. Sun and N. Sepehri, "Impedance Control of a Teleoperated Pneumatic Actuator: Implimentation and Stability Analysis," *Control and Intelligent Systems,* vol. 45, no. 1, pp. 19-30, 2017.

[32] J. Han, "Auto-disturbance rejection control and its applications," *Control and Decision,* vol. 13, no. 1, pp. 19-23, 1998.

[33] Z. Gao, "Active disturbance rejection control: A paradigm shift," in *Proceedings of the American Control Conference*, Minneapolis, 2006.

[34] L. Dong, A. Mandali, A. Morinec and Y. Zhao, "Active Disturbance Rejection Based Load Frequency Control and Voltage Regulation in Power Systems," *Control Theory and Technology,* vol. 16, no. 4, pp. 336-350, 2018.

[35] J.-J. E. Slotine and W. Li, Applied Nonlinear Control, Upper Saddle River, New Jersey: Prentice-Hall, Inc., 1991.

[36] S. Shao and Z. Gao, "On the Conditions of Exponential Stability in Active Disturbance Rejection Control Based on Singular Perturbation Analysis," *International Journal of Control,* vol. 90, no. 10, pp. 1103-1116, 2017.

[37] J. Y. Hung, W. Gao and J. C. Hung, "Variable Control Structure: A Survey," *IEEE Transactions of Industrial Electronics,* vol. 40, no. 1, pp. 2-22, 1993.

[38] C. Pu, J. Ren and J. Su, "The Sliding Mode Control of the Drum Water Level Based on Extended State Observer," *IEEE Access,* vol. 4, pp. 135942-135948, 2019.

APPENDIX A

PNEUMATIC ACTUATOR SIMULINK MODEL

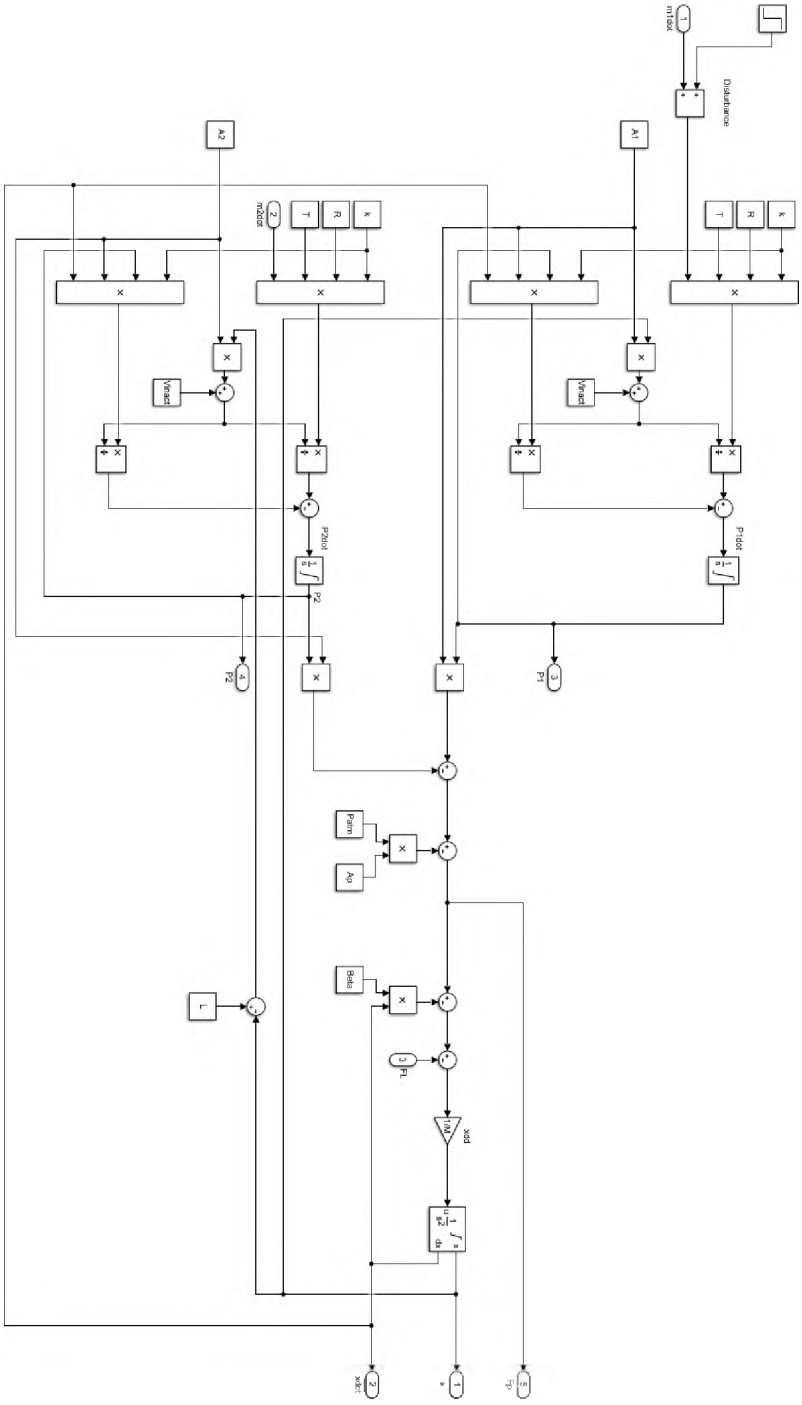

APPENDIX B

IMPEDANCE CONTROL MASS SPRING DAMPER MODEL

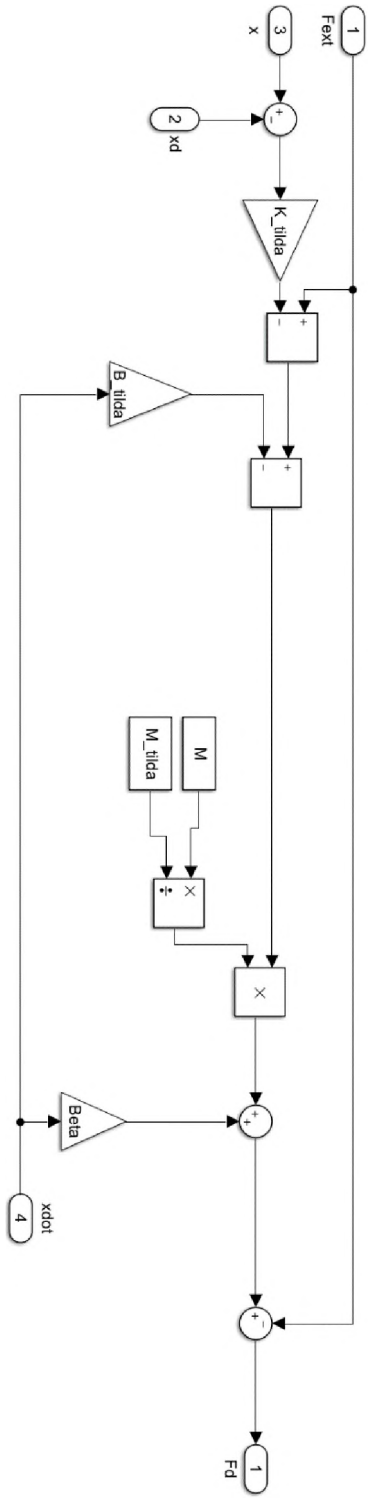

APPENDIX C

IMPEDANCE CONTROL FORCE TO PRESSURE MODEL

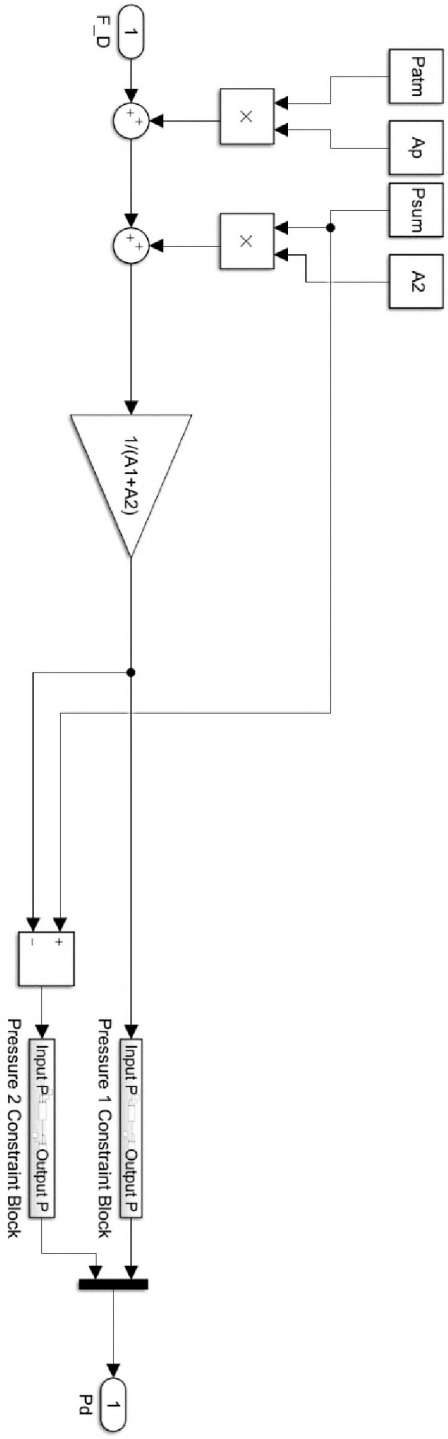

APPENDIX D

ADRC SIMULINK MODEL

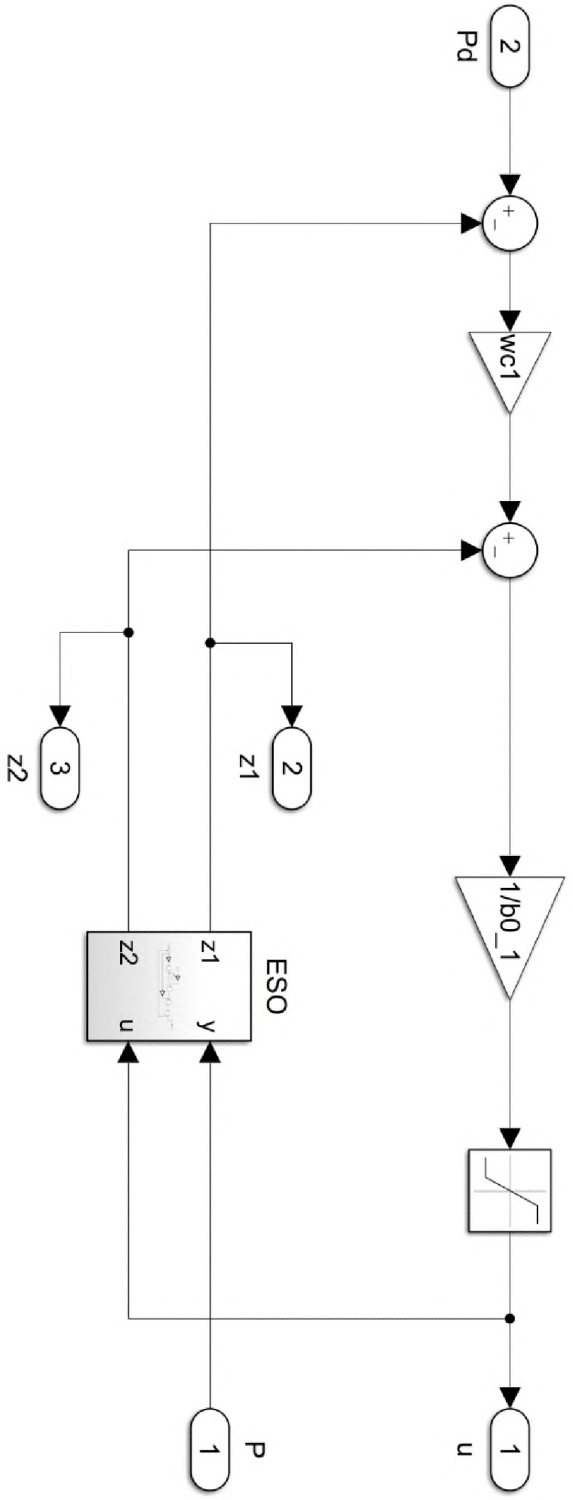

APPENDIX E

ESO-BASED SMC MODEL

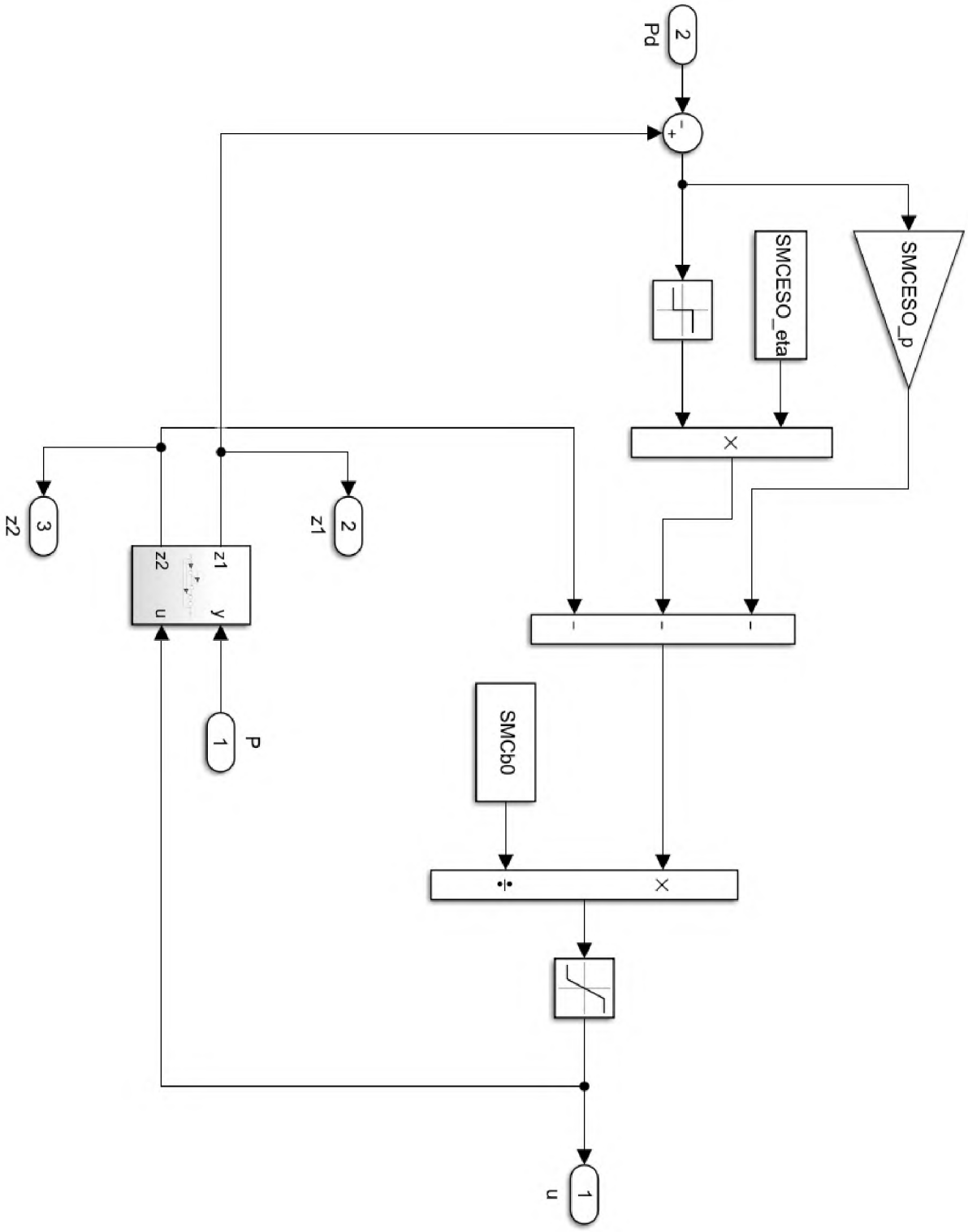

APPENDIX F

SMC SIMULINK MODEL